# UNIVERSITY OF GENOVA

**POLYTECHNIC SCHOOL**

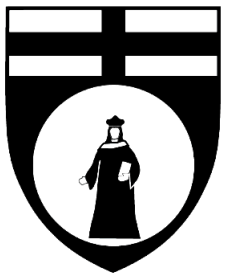

**DIBRIS**

Department of Informatics, Bioengineering, Robotics,
and Systems Engineering


MASTER OF SCIENCE THESIS

IN

REHABILITATION ENGINEERING AND BIOMATERIALS

# Numerical simulations of particles deposition on the cornea


**Candidate**

Alessandro Barbero

**Supervisors**

Prof. Ing. Rodolfo Repetto  Prof. Ing. Jan Oscar Pralits


March 2021

# Abstract

The purpose of this thesis is to study how the ocular surface is protected from the attack of pathogens present daily in the air of cities. This function is performed by physiological structures the role of which has not been studied in depth so far: the eyelashes. To understand in detail how these structures work, we have created a realistic geometry of the surface of face and eye. The first part of this thesis involved the CAD realization of a 3D model of a human face, necessary to simulate how the flow fields generated could be influenced by the different anatomical structures. To make the study as complete as possible we have made four different models that differ from each other in the length of the eyelashes. The second part of the work consists in numerical simulation of the motion of fluid and particles. We have chosen, as a case study, a running person (at a speed of 3.5 $m/s$) in a polluted area. The particles considered are of variable micrometric dimensions, in order to make our study parametric and recreate a possible scenario of atmospheric pollution present in cities due to emissions of both natural and anthropogenic origin.
We found that the role of eyelashes in terms of defense of the ocular surface is effectively visible both because this structure modifies the flow field near the eye and because eyelashes act like a sieve and trap particles. In particular we have seen how the tendency to intercept particles by the eyelashes grows as their length increases, with a similar trend with particles of different diameters. The conclusions drawn are useful for interpreting the role of the eyelashes in protecting the ocular surface.

# Sommario

Lo scopo di questa tesi è studiare come la superficie oculare sia protetta dall'attacco di agenti patogeni presenti quotidianamente nell'aria delle città. Questa funzione è svolta da strutture fisiologiche il cui ruolo non è stato finora studiato in profondità: le ciglia. Per capire in dettaglio come funzionano queste strutture, abbiamo creato una geometria realistica della superficie del viso , degli occhi e delle ciglia. La prima parte di questa tesi ha riguardato la realizzazione CAD di un modello 3D di un volto umano, necessario per simulare come i campi di flusso generati potessero essere influenzati dalle diverse strutture anatomiche. Per rendere lo studio il più completo possibile abbiamo realizzato quattro diversi modelli che differiscono tra loro per la lunghezza delle ciglia. La seconda parte del lavoro consiste nella simulazione numerica del moto di fluidi e particelle. Abbiamo scelto, come caso di studio, una persona che corre (alla velocità di 3,5 $m/s$) in un'area inquinata. Le particelle considerate sono di dimensioni micrometriche variabili, al fine di rendere parametrico il nostro studio e ricreare un possibile scenario di inquinamento atmosferico presente nelle città dovuto ad emissioni sia di origine naturale che antropica. Abbiamo scoperto che il ruolo delle ciglia in termini di difesa della superficie oculare è effettivamente visibile sia perché questa struttura modifica il campo di flusso vicino all'occhio sia perché le ciglia agiscono come un setaccio e intrappolano le particelle. In particolare abbiamo visto come cresca la tendenza ad intercettare le particelle da parte delle ciglia all'aumentare della loro lunghezza, con un andamento simile con particelle di diverso diametro. Le conclusioni tratte sono utili per interpretare il ruolo delle ciglia nella protezione della superficie oculare.

# Contents

# Chapter 1

# Introduction

The eye is responsible for the trasmission of many diseases [1]. These have different vectors of propagations such as: virus, fungal and bacteria. The atmospheric particulate matter is a factor that eases the trasmission.
The acronym PM stands for "Particulate Matter" and is used to indicate fine particles, composed of microscopical parcels, solid and liquid, of different nature and chemical composition, which are found in suspension in the air that we breathe. According to their dimension we conventionally distinguish the fine particles in PM10, PM2.5 and PM1 where the number after PM stands for the size of the parcels diameter. More specifically PM10 identifies one of the parts in which Particulate Matter is classified, those whose aerodynamic diameter (corresponding to the diameter of a sphere of $1 g/cm^3$ of density that falls in the air at the same speed of the considered parcel) is between $10\mu$ and $2,5\mu$. For a better comprehension of the sizes we are referring to, we can consider that a cobweb has a thickness of $7\mu$ [2].

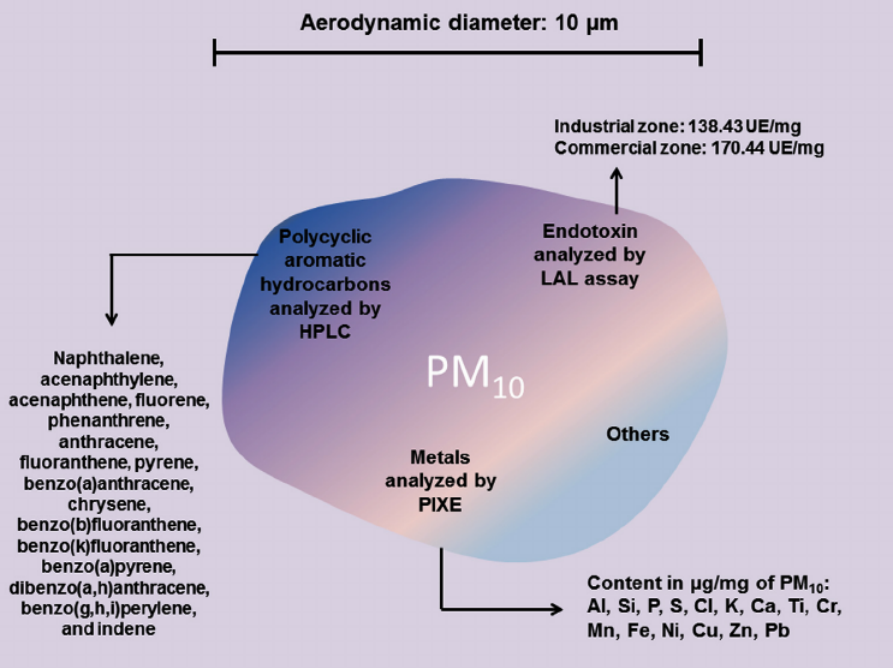


Figure 1.1: *Representation of PM10*

Many studies have found a correlation between the spread of breathing infections and the rate of Particulate Matter in the air [3]. These researches get relevance in the context of the Sars-CoV2 pandemic broke out in March 2020 in China. This virus has recently been identified as an infectious disease that affects humans respiratory system. The disease is caused by Sars-CoV2 that has been identified in chinese patients with severe pneumonia and flu-like symptoms. COVID-19 is a contagious illness that spreads rapidly via droplets parcels resulting from the action of an infected person's sneezing and coughing [4]. Also in this case, some studies have highlighted the correlation between the air pollution and the larger spread of the epidemic [5].
These considerations concerned not only China but the entire world. Even in Italy, some studies highlighted the impact of air pollution during the development of pandemic [6]. In fact has been underlined how between January and April 2020 the spreading of the virus has been affected from the higher rate of particulate in the metropolitan area of Milan.

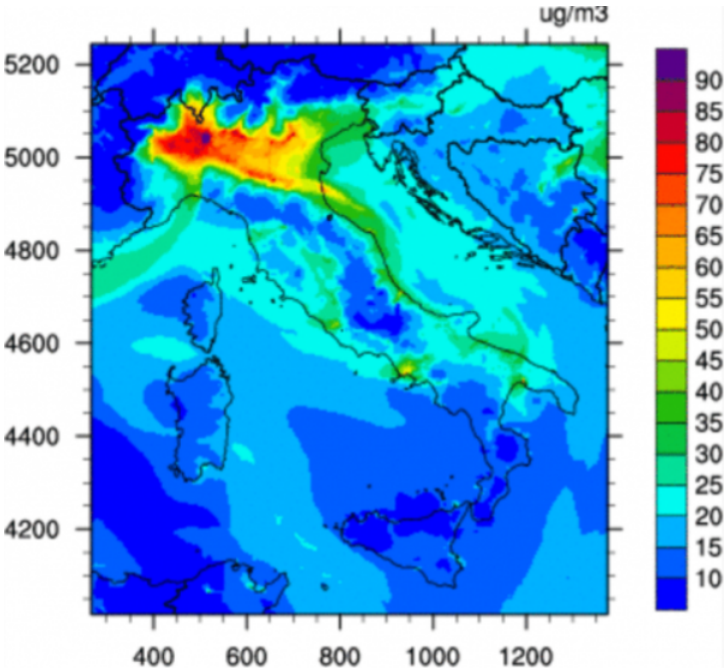


Figure 1.2: *Representation of PM10*

Starting from these data we have chosen to study the role of atmospheric particulate in the spread of infectious diseases through the eye. We chose to use three different size of particles: The first with variable diameter according to a normal distribution, the second with a fixed diameter of 50 $\mu m$ and the third with a fixed diameter of 100 $\mu m$. We have chosen to make ours a parametric study with the aim of broadening the range of situations that can be analyzed.

The estimates derived from these results can also be applied to assessments relating to PM10. This is very important because PM10 is considered one of the main marker of the air quality and is characterized by long periods of stay in the atmosphere, it can be carried even to big distance from the inlet point and it has a complex and variable chemical nature depending on the features of the territory, of the presence of factories, of the fuel used, of climate and of all those factors that determine their formation. Furthermore, many chemical substances, such as polycyclic aromatic hydrocarbons (PHAs) and metals (such as lead, nickel, cadmium, arsenic, vanadium, chromium), can stick to the surface of fine particles causing effetcs on exposed population's health. According to ISPRA [7] "particulate is the fine particle with biggest impact on human health. Various epidemiological

studies on the health effects of particulate air pollution, have shown associations between mass concentrations of PM10 and an increase of both mortality and hospitals admissions for heart and respiratory diseases in the population".
Since the eye can be source of infection transmission, it has some defensive mechanisms. It is commonly believed that the eye's only line of defence is its sophisticated tear duct system which provides a thin composite layer of mucus, oil and water to lubricate the eyelid, hydrate the cornea and remove particles deposited onto the eye [8]. Instead, little is said about others defensive mechanisms of the eye, like for example eyelashes. For this reason we chose to study defensive function of eyelashes, observing how it varies as the length of the eyelashes varies. This is because it is one of the most important parameter that varies between the ethnic groups of the human race [9].

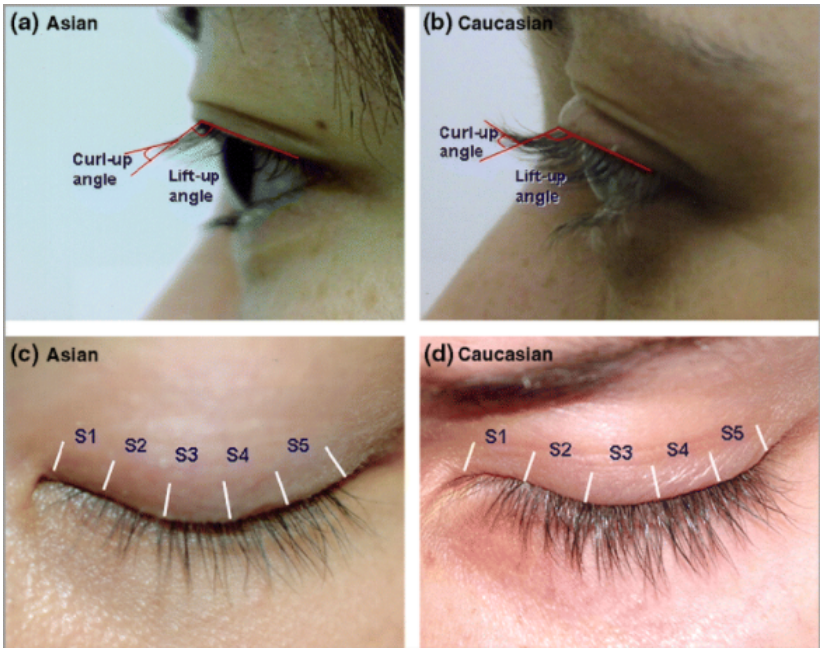


Figure 1.3: *Different eyelashes lengths in different ethnic groups*

In this way our sample will be as complete and varied as possible. Furthermore, it is proved that the variance from the eyelashes' length from its optimal length can create problems for the natural functioning of the entire ocular system: short eyelashes create a stagnation zone above the ocular surface that thickens the boundary layer, causing shear stress to decrease with increasing eyelash length. Long eyelashes channel flow towards the ocular surface, causing shear stress to increase with increasing eyelash length. These competing effects result in a mini-

mum shear stress for intermediate eyelash lengths [1].
The aim of this study is therefore to investigate the actual defense role that the eyelashes play and how this can change, for better or for worse, depending on the variation of the length parameter.

# Part I

# Case of Study and Numerical Tools

# Chapter 2

# Eye and Eyelashes

## 2.1 Anatomical Structure of the Eye

The eyes are among the most important organs in the body. The human eye measures approximately 22 to 27 mm in anteroposterior diameter and 69 to 85 mm in circumference. The human eyeball consists of three primary layers, with each of those three layers being further subdividable [10].

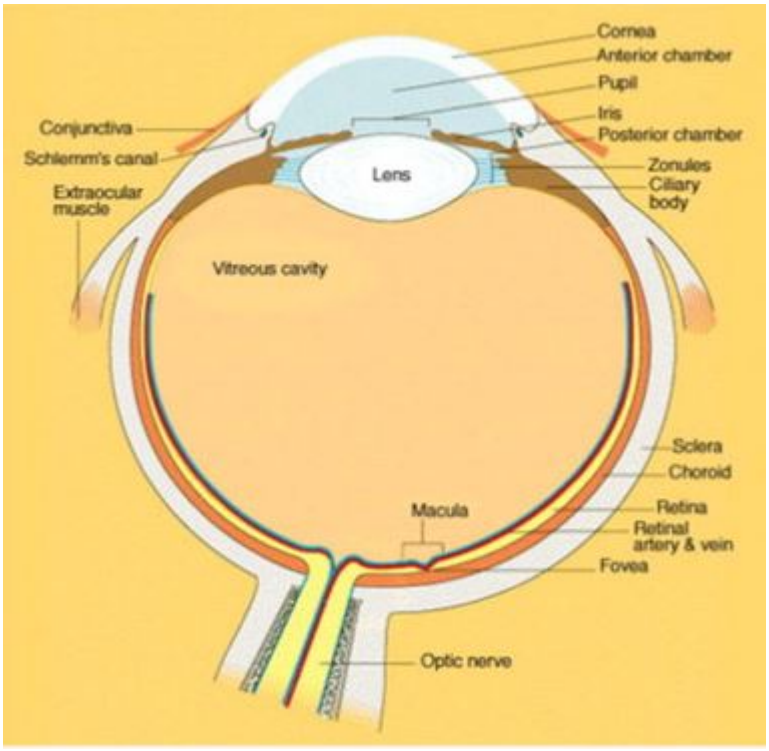


Figure 2.1: *Pictures of eye anatomical structure*

The three primary layers and their respective subdivisions include:

- the outermost supporting layer of the eye, which consists of clear cornea, opaque sclera, and their zone of interdigitation, designated as the limbus
- the middle uveal layer of the eye, constituting the central vascular layer of the globe, which encompasses the iris, ciliary body, and choroid
- the interior layer of the eye, commonly designated as the retina

The human globe is compartmentalized into three distinct chambers: the anterior chamber, the posterior chamber, and the vitreous cavity. The anterior chamber is formed anteriorly by the posterior aspect of the cornea, posteriorly by the anterior aspect of the iris and crystalline lens, and peripherally by the anterior chamber drainage angle. The posterior chamber is demarcated anteriorly by the posterior surface of the iris, posteriorly by the anterior surface of the zonular fibers, centrally by the crystalline lens, and peripherally by the ciliary processes. The vitreous chamber is delineated anteriorly by the zonular fibers, the ciliary

body, and the posterior aspect of the crystalline lens and posteriorly by the optic nerve and retina.

## 2.2 Eyelashes Anatomical Structure

The eyelids are formed by reinforced folds of skin that are attached to the thin skeletal muscles which permit movement. The orbicularis oculi muscle assists in the control of the eyelids, and it receives additional assistance from the levator palpebrae superioris muscle, which is designated to the upper eyelid and explains why the upper lid has more movement options than the lower lid [11]. When the eyelids draw down over the eye, or the eyes "close", it is the result of the orbicularis oculi muscle contracting. When the levator palpebrae superioris muscle contracts, the result is the "opening" of the eye, or the eylid drawing back up over the eye to reveal the eyeball. The eyeball is protected by the eyelid, both from desiccation and from impalement. When the eyelid blinks, which occurs every 7 seconds or so, fluid flushes the eyeball and keeps it moisturized. The eyelid also reflexively blinks when the eye senses a particle that threatens to enter it. The eyelid will usually blink reflexively when the eye is adjusting to a new line of vision to help prevent the initial blurry vision that can occur from refocusing too quickly. The small but detectable space between the upper and the lower eyelid is known as the palpebral fissure. When the eyes are closed, this fissure appears to be nothing more than a line of connection. When the eyes are open, the fissure takes on an elliptical shape. The small medial and lateral angles where the eyelids conjoin is known as the commissure of the eye. The medial commissure is the larger of the two, and is noted by a small elevation of red flesh which is known as the lacrimal caruncle. The lacrimal caruncle is responsible for creating white secretions that get caught at the corner of the eye, usually during sleep, thank to the sebaceous and sudoriferous glands. The last forms of secretion protection available for the eyelids are the modified sweat glands known as ciliary glands. All of these glands help to keep proper moisture in the eye and permit smooth eye movements and operation. If one of the sebaceous glands becomes infected, this is commonly referred to as a sty. Each eyelid is the perfect anchoring ground for eyelashes, one row per eyelid. Eyelashes are the structures that grow at the edge of the eyes. Eyelashes have a specific function, that of protecting the eyes from impurities. They have an acute sensitivity in perceiving the presence of foreign bodies that

approach the eyes and therefore, by reflex, involuntarily activate their closing and opening. Each single eyelash is embedded into the eyelid by the root, which anchors into a root hair plexus. This gives the eyelash hairs additional sensitivity to snap the eye closed in the event of an airborne particle reaching the eye. The eyelashes belonging to the upper lids and the lower lids vary from each other. The upper lid eyelashes are longer, tend to curve in an upward direction, and are more noticeable than the lower lid eyelashes, which are shorter and tend to be stumpy without much curve. In the eyes there is the "tear film", which has the function of cleaning the eyes of any impurities, distributing itself over the entire sclera [8]. The eyelashes, opening and closing, help the "tear film" to distribute itself equally over the entire ocular sclera, thus promoting complete and continuous hydration.

## 2.3 Cad Geometry

The description of the geometry of the CAD model turns out to be central to implement the Computational Fluid Dynamic (CFD) study that we want to perform. The main software that we have been used to realize this model is Blender, as it will be explained in the next chapter. The first step to deal with the CFD case is to create a geometrical domain within which to develop the simulations. Afterwards, the geometrical model is built and it consists, in this case, in the reproduction of a human face. These steps are shown in the *Figures* 2.2, 2.3:

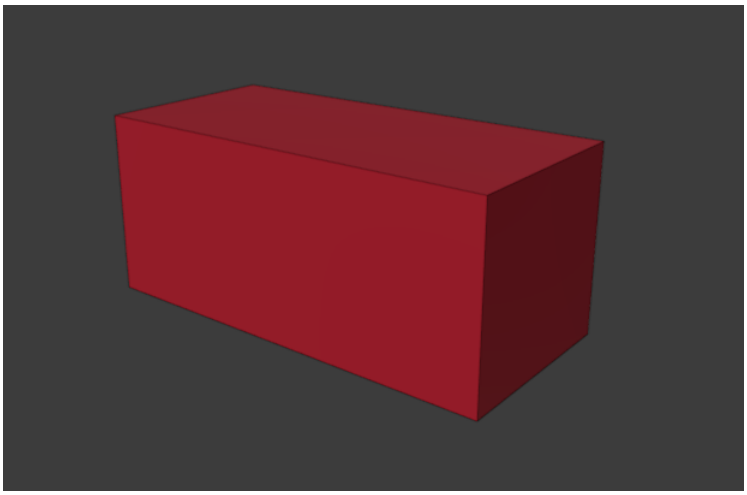

Figure 2.2: *Simulation domain created with Blender*

Figure 2.3: *Human face created with Blender*

The following section describes all the assumptions that has been made when going from the reality to the aerodynamic model of the eye and eyelashes. The basic guideline in this process of geometrical modelling is to keep the model as close as possible to the reality without forgiving that CFD can be extremely time consuming.
The geometric domain within which we work is a parallelepiped of dimensions $35cm \times 35cm \times 75cm$. The surfaces delimiting the calculation volume have been named as follows:

- Bottom
- Top
- North
- South
- East
- West

Intersected with it, precisely with the West, North and Top faces, we find the surface of the three-dimensional face, as shown in the *Figure* 2.4:

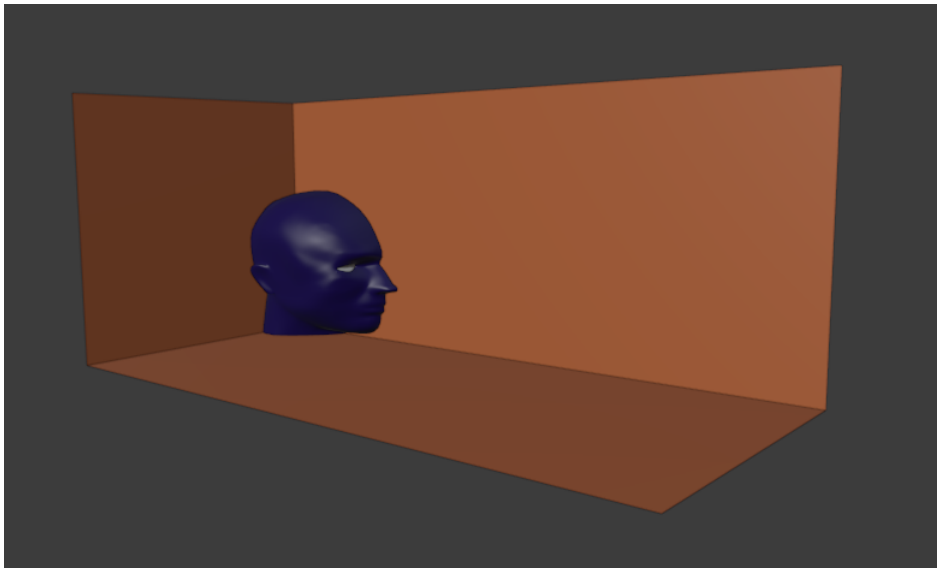

Figure 2.4: *Human face intersected with the domain created with Blender*

During numerical simulations, Bottom represents the inlet, contrariwise Top, intersected with the face's surface, represents the arrival point of the particles. In some previous studies the eye geometry was simpler because it wasn't considered as indispensable to create a considerable of CFD model. In this case we assume it might be interesting notice how the various face elements geometry could interfere changing the parcel flux towards the eye. Another aspect that we have focused on is the geometry of the eyelashes. Often these, in some previous works, were represented as simple cylinders. In this study, however, we tried to make them more realistic: in first place we introduced a curvature, in order to reproduce the real trend of the eyelashes; in second place, the end of the eyelashes were sharpened to respond to a standard of greater likelihood with the real model. The result is shown in *Figure* 2.5:

Figure 2.5: *Eyelashes created with Blender*

Because of the variation of eyelashes number and lenght in different ethnic groups, various geometric models have been created. The parameters that could have been accounted for were: lenght, diameter's dimension and the overall number of eyelashes. In this case we assumed it might be proper focus exclusively on the lenght, the parameter that we thought could have led to more significative results. On this purpose we created four geometric models that differ for eyelashes' lenght. The eyelash lengths are respectively:

- model 1: 0 mm
- model 2: 3.3 mm
- model 3: 6.6 mm
- model 4: 1 cm

As we can see in *Figure* 2.6:

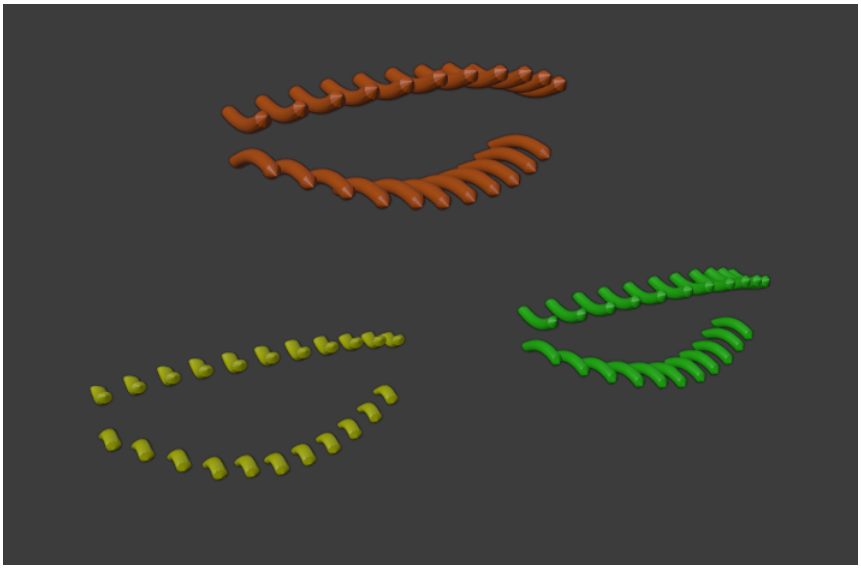

Figure 2.6: *Eyelashes created with Blender. The different colors indicate the different lengths: 3.3 mm in yellow, 6.6 mm in green and 1 cm in orange*

# Chapter 3

# Open Source Tools

## 3.1 Blender

Blender is the free and open source 3D creation suite. It supports the entirety of the 3D pipeline-modeling, rigging, animation, simulation, rendering, compositing and motion tracking, video editing and 2D animation pipeline [12]. These features make it a very versatile and widely used program given its large size flexibility. The possibility of importing and exporting models, helps the interaction with other programs and the reusability of the work done, given the great compatibility with other platforms. Blender's physics system allows to manipulate elements by simulating even the liquid or gaseous state, also managing collisions and gravity. The program, as well to the great potential, offers the programmer a great deal of tools, which allow to learn how to create a model in a simple and intuitive way, leaving transparent some aspects of modeling.
3D modelling means a process that allows you to create an object, called a model, within a defined virtual space. Solid modeling is based on using solid primitives that come modified and shaped little by little until you reach the shape you want. Every object corresponds to a specific geometric pattern consisting of several lines e points. Each shape can therefore be expressed as a particular polygon, whose principal components are vertices, edges and faces, in detail:

- `vertices`: they are a single point in 3D space, used as extreme of an edge.
- `edges`: they are segments delimited by two vertices. These are crucial to create the faces and increase the detail of the modeled objects.

- `faces`: They are planes, identified by at least 3 edges. They are used for create solid objects which will then be shown to the user.

In this thesis, this tool has been used to create the geometry of various cases, changing the dimensional parameters of the eyelashes on a case-by-case basis.

## 3.2 OpenFOAM

OpenFOAM *Open Source Field Operation And Manipulation*) is an open source software for computational fluid dynamics (CFD), that can be used to build a variety of computational solvers for problems in continuum mechanics with a focus on finite volume discretization. It's owned by the OpenFOAM Foundation and distributed exclusively under the General Public Licence (GPL). The GPL gives users the freedom to modify and redistribute the software and a guarantee of continued free use [13]. OpenFOAM is first and foremost a C++ library, used primarily to create executables, known as applications. The applications fall into two categories: solvers, that are each designed to solve a specific problem in continuum mechanics; and utilities, that are designed to perform tasks that involve data manipulation. New solvers and utilities can be created by its users with some pre-requisite knowledge of the underlying method, physics and programming techniques involved [14]. OpenFOAM is supplied with pre- and post-processing environments. The interface to the pre- and post-processing are themselves OpenFOAM utilities, thereby ensuring consistent data handling across all environments. The overall structure of OpenFOAM is shown in *Figure* 3.1

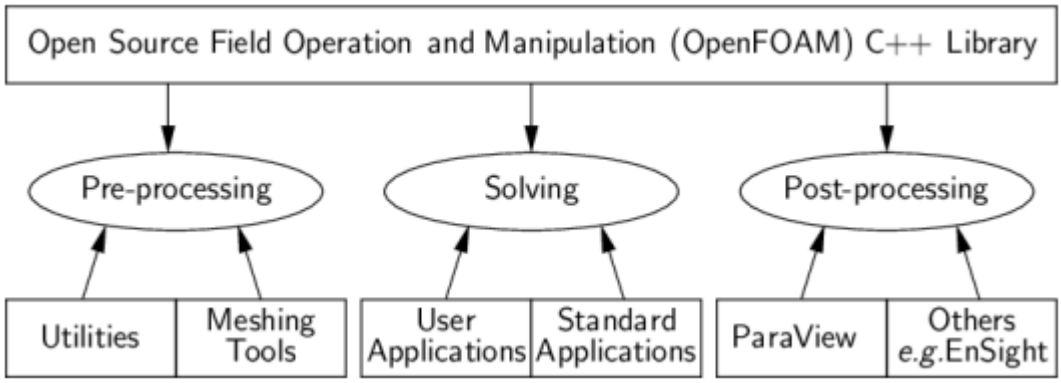


Figure 3.1: *Overview of OpenFOAM structure*

At the core of these libraries are a set of object classes that allow the programmer to manipulate meshes, geometries, and discretization techniques at a high level of coding. *Tables* 3.2 3.3 3.4 3.5 present a list of the main OpenFOAM classes and their functions. These classes represent the basic bricks for the development of OpenFOAM based applications and utilities. They enable programmers constructing a variety of algorithms while allowing for extensive code re-use.

| Objects | Type of data | OpenFOAM® Class |
|---|---|---|
| Interpolation | Differencing schemes | surfaceInterpolation<template> |
| Explicit discretization: differential operator | ddt, div, grad, curl | fvc:: |
| Implicit discretization: differential operator | ddt, d2dt2, div, laplacian | fvm:: |

Figure 3.2: *Numerics and discretizations*

| Objects | Type of data | OpenFOAM® Class |
|---|---|---|
| Variables | Primitive variables | scalar, vector, tensor |
| Mesh components | Point, face, cell | point, face, cell |
| Finite volume mesh | Computational mesh | fvMesh, polyMesh |
| Time | Time database | Time |

Figure 3.3: *Computational domain*

| Objects | Type of data | OpenFOAM® Class |
|---|---|---|
| Field | List of values | Field<template> |
| Dimensions | Dimension set up | dimensionSet |
| Variable field | Field + mesh + boundaries + dimension | GeometricField<template> |
| Algebra | +, −, pow, = , sin, cos… | field operators |

Figure 3.4: *Field operation*

| Objects | Type of data | OpenFOAM® Class |
|---|---|---|
| Sparse matrix | Matrix coefficients and manipulation | lduMatrix, fvMatrix |
| Iterative solver | Iterative matrix solvers | lduMatrix::solver |
| Preconditioner | Matrix preconditioner | lduMatrix::preconditioner |

Figure 3.5: *Linear equations systems and linear solvers*

OpenFOAM therefore has a wide range of functions to simulate anything from turbulent flows in fluid dynamics to fires and fire suppression in buildings, involving combustion, chemical reactions, heat transfer, liquid sprays and films. It includes tools for meshing in and around complex geometries, and for data processing and visualisation, and more. Almost all computations can be executed in parallel as standard to take full advantage of today's multi-core processors and multi-processor computers. From the official website, some of the main features are listed below:

- FLUID DYNAMICS PHYSICAL MODELLING
  - Turbulence modelling: Large-Eddy Simulation (LES) and Detached-Eddy Simulation (DES, DDES, etc)
  - Thermophysical modelling
  - Transport/rheology
  - Multiphase flows
  - Rotating flows with multiple reference frames (MRF)
  - Rotating flows with arbitrary mesh interface (AMI)
  - Dynamic meshes
  - Compressible/thermal flows
  - Conjugate heat transfer
  - Porous media
  - Lagrangian particle tracking
  - Reaction kinetics / chemistry
- GEOMETRY AND MESHING
  - Mesh generation for complex geometries with snappyHexMesh
  - Mesh generation for simple geometries with blockMesh
  - Mesh conversion tools
  - Mesh manipulation tools
- DATA ANALYSIS

  - ParaView post-processing
  - Post-processing command line interface (CLI)
  - Graphs and data monitoring

- NUMERICAL SOLUTION
  - Numerical method
  - Linear system solvers
  - ODE system solvers

- COMPUTING AND PROGRAMMING
  - Equation syntax
  - Libraries of functionality
  - Parallel computing

### 3.2.1 Case Structure

The basic directory structure for a OpenFOAM case, that contains the minimum set of files required to run an application, is shown in *Figure* 3.6 and described as follows:

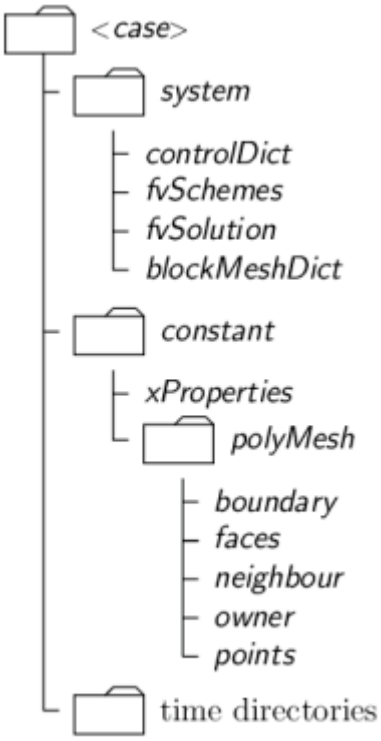


Figure 3.6: *Structure of an OpenFOAM case*

Below is the description of the main directories contained in the case structure:

- `system`: This directory is necessary for setting parameters associated with the solution procedure itself. It contains at least the following 3 files:
  - `controlDict`: run control parameters are set including start/end time, time step and parameters for data output.
  - `fvSchemes`: discretisation schemes used in the solution may be selected at run-time.
  - `fvSolution`: the equation solvers, tolerances and other algorithm controls are set for the run.
- `constant`: This directory includes a folder (`polyMesh`) which contains a complete description of the mesh and folders that contain information about the development of the physics of the system (gravity, turbulence properties, etc.)

- `time directories`: It contains individual files of data for particular fields. The data can be: either, initial values and boundary conditions that the user must specify to define the problem; or, results written to file by OpenFOAM.

We could talk about how OpenFOAM is structured, but this is not the goal of this thesis. For further details the CFD direct website [13] is suggested.

### 3.2.2 The Programming Language

*C++* is an *Object-Oriented Programming* language that attempts to provide techniques for managing complexity, achieving the aim of the reuse of software components. The key mechanism of object technology are encapsulation, polymorphism and inheritance [15].

#### Encapsulation

Encapsulation is the mechanism by which related data and procedures are bound together within an object. In effect, an object is a software capsule that functions as a black box, responding to messages from other objects and dispatching messages of its own in ways that do not reveal its internal structure. In this way, encapsulation supports and extends the proven principle by information hiding. Information hiding is valuable because it prevents local changes from having global impact. In the case of objects, it allows the implementations of individual objects to be altered without affecting the way these objects communicate through messages.

#### Inheritance

Inheritance is the mechanism that allows classes to be defined as special cases, or subclasses, of eachother. If a *department* class is declared to be a subclass of *organization*, the *department* class automatically encorpartes all the methods and variables defined in the *organization* class. Inheritance can cascade down over a number of levels, allowing deeply nested *class hierarchies* to be constructed.

#### Polymorphism

The fact that different objects can respond to the same message in different ways is known as *polymorphism*, a Greek term meaning "many forms". The power of

polymorphism is that it greatly simplifies the logic of programs. A requestor no longer has to us nested IF statements or complex CASE statements to call the appropriate procedure. Instead, the proper procedure is automatically invoked sending the request to a particular object.
polymorphic messaging has several advantages over conditional execution logic:

- It is much shorter, reducing the size and complexity of the resulting program code.
- It executes faster because the program code compiles down to a direct jump to the appropriate procedure rather than passing through real-time sieve to identify that procedure.
- It is more flexible in that new financial instruments can be added or old ones removed without having to rewrite the selection logic.

# Part II

# Fluid Dynamics Characterization of Eye and Eyelashes

# Chapter 4

# Governing Equations

## 4.1 Conservation Laws

The principle of conservation states that for an isolated system certain physical measurable quantities are conserved over a local region. This conservation principle or conservation law is an axiom that cannot be proven mathematically but can be expressed by a mathematical relation. Laws of this type govern several physical quantities such as mass, momentum, and energy (the Navier-Stokes equations). The conservation laws involving fluid flow and related transfer phenomena can be mathematically formulated following either a Lagrangian (material volume, MV) or an Eulerian (control volume) approach. In the Lagrangian specification of the flow field, the fluid is subdivided into fluid parcels and every fluid parcel is followed as it moves through space and time. On the other hand, the Eulerian approach focuses on specific locations in the flow region as time passes [16].
Assuming a continuous phase the most common method of describing fluid flow is the fixed reference system Eulerian approach that is synthetically presented below. A short description of the Lagrangian method will be introduced in the next section.

### 4.1.1 Continuity Equations

The principle of conservation of mass indicates that in the absence of mass sources and sinks, a region will conserve its mass on a local level [16].
Assuming $\rho$ as density, applying the Reynolds transport theorem, the general

expression for conservation of mass as applied to a control volume will be:

$$\int_V \frac{\partial \rho}{\partial t}\, dV + \int_S \rho \mathbf{V} \cdot \mathbf{n}\, dS = 0 \tag{4.1}$$

where $S$ is the surface of the control volume $V$ . Thanks to the divergence theorem - and noticing that the conservation of mass should be respected for every control volume - this equation can be written in a differential form, called the continuity equation:

$$\frac{\partial \rho}{\partial t} + \nabla \cdot (\rho \mathbf{V}) = 0. \tag{4.2}$$

### 4.1.2 Conservation of Linear Momentum

The principle of conservation of linear momentum indicates that in the absence of any external force acting on a body, the body retains its total momentum, i.e., the product of its mass and velocity vector. Since momentum is a vector quantity, its components in any direction will also be conserved [16].
The conservative version is obtained by applying the form of the Reynolds transport and of divergence theorems, and is written as:

$$\rho \frac{\partial \mathbf{v}}{\partial t} + \nabla \cdot (\rho \mathbf{v} \otimes \mathbf{v}) = \mathbf{f}. \tag{4.3}$$

Where $\mathbf{f} = \mathbf{f}_\mathrm{s} + \mathbf{f}_\mathrm{b}$ is the sum of the external surface forces $\mathbf{f}_\mathrm{s}$ and body forces $\mathbf{f}_\mathrm{b}$ acting on the control volume.

#### Surface forces

For the arbitrary macroscopic volume element, the forces acting on its surface are due to pressure and viscous stresses which can be expressed in term of the total stress tensor:

$$\boldsymbol{\sigma} = \begin{pmatrix} \sigma_{xx} & \tau_{xy} & \tau_{xz} \\ \tau_{yx} & \sigma_{yy} & \tau_{yz} \\ \tau_{zx} & \tau_{zy} & \sigma_{zz} \end{pmatrix} = \begin{pmatrix} -P & 0 & 0 \\ 0 & -P & 0 \\ 0 & 0 & -P \end{pmatrix} + \begin{pmatrix} \tau_{xx} & \tau_{xy} & \tau_{xz} \\ \tau_{yx} & \tau_{yy} & \tau_{yz} \\ \tau_{zx} & \tau_{zy} & \tau_{zz} \end{pmatrix} = -p\boldsymbol{I} + \boldsymbol{\tau}, \tag{4.4}$$

where $\boldsymbol{I}$ is the identity tensor, $p$ the pressure and $\boldsymbol{\tau}$ is the deviatoric viscous stress tensor. The pressure is the negative part of the mean of the normal stresses and is given by:

$$p = -\frac{1}{3}(\sigma_{xx} + \sigma_{yy} + \sigma_{zz}). \tag{4.5}$$

Hence the surface force acting on a differential surface element $dS$ is:

$$\int_S \mathbf{f_s}\, dS = \int_A \boldsymbol{\sigma} \cdot \mathbf{n}\, dA = \int_V \nabla \cdot \boldsymbol{\sigma}\, dV \longrightarrow \nabla \cdot \boldsymbol{\sigma} = -\nabla p + (\nabla \cdot \boldsymbol{\tau}). \tag{4.6}$$

**Body forces**

The main Body forces are given below:

- Gravitational forces $\mathbf{f_b} = \rho\mathbf{g}$, due to the presence of a gravitational field
- Coriolis and centrifugal forces, respectively $\mathbf{f_b} = -2\rho(\boldsymbol{\omega}\times\mathbf{v}) - \rho(\boldsymbol{\omega}\times(\boldsymbol{\omega}\times\mathbf{r}))$, due to a rotating frame of reference

Hence introducing the expressions of surface and body forces in Eq. (4.3) the general conservative form of the momentum equation is obtained as:

$$\rho\frac{\partial \mathbf{v}}{\partial t} + \rho\nabla \cdot (\mathbf{v} \otimes \mathbf{v}) = -\nabla p + (\nabla \cdot \boldsymbol{\tau}) + \mathbf{f_b}$$

(4.7)

To procede further the type of fluid should be specified in order to relate $\boldsymbol{\tau}$ with the other flow variables. For a Newtonian fluid the stress tensor is a linear function of the strain rate and is given by:

$$\boldsymbol{\tau} = \mu(\nabla \boldsymbol{v} + (\nabla \boldsymbol{v})^T) + \lambda(\nabla \cdot \mathbf{v})\mathbf{I}, \tag{4.8}$$

where $\mu$ is the molecular viscosity, $\lambda$ the bulk viscosity coefficient usually set equal to $\lambda = \frac{2}{3}\mu$. Taking the divergence of Eq.(4.8) and substituting in Eq.(4.1.2) the final conservative form of the momentum equation for Newtonian fluids becomes also called Navier-Stokes equation:

$$\rho\frac{\partial \mathbf{v}}{\partial t} + \rho\nabla \cdot (\mathbf{v} \otimes \mathbf{v}) = \nabla \cdot (\mu\nabla \boldsymbol{v}) - \nabla p + \nabla \cdot (\mu(\nabla \mathbf{v^T})) + \nabla(\lambda\nabla \cdot \mathbf{v}) + \mathbf{f_b}. \tag{4.9}$$

For incompressible flows the divergence of velocity vector is zero, $\nabla \cdot \mathbf{v} = \mathbf{0}$, and for constant molecular viscosity the momentum equation can be further simplified:

$$\rho\frac{\partial \mathbf{v}}{\partial t} + \rho\nabla \cdot (\mathbf{v} \otimes \mathbf{v}) = -\nabla p + \mu\nabla^{\mathbf{2}}\mathbf{v} + \mathbf{f_b} \tag{4.10}$$

### 4.1.3 Conservation of Energy

The conservation of energy is governed by the first law of thermodynamics which states that energy can be neither created nor destroyed during a process; it can only change from one form (mechanical, kinetic, chemical, etc.) into another. Consequently, the sum of all forms of energy in an isolated system remains constant [16].
Considering a material volume of mass $m$, density $\rho$, and moving with a velocity $v$. Defining the total energy $E$ of the material volume at time $t$ as the sum of its internal and kinetic energies, then $E$ can be written as:

$$E = m(\hat{u} + \frac{1}{2}\mathbf{v} \cdot \mathbf{v}) \tag{4.11}$$

where $\hat{u}$ is the internal energy per unit mass. The first law of thermodynamic states that the rate of change of the total energy of the material volume is equal to the rate of heat addition and work extraction through its boundaries:

$$\left(\frac{dE}{dt}\right)_{MV} = \dot{Q} - \dot{W}. \tag{4.12}$$

The net rate of heat transferred to the material element $\dot{Q}$ is the sum of two components. The first component is the rate transferred across the surface of the element $\dot{Q_S}$ and the second generated/destroyed (e.g., due to a chemical reaction) within the material volume $\dot{Q_V}$. Moreover, the net rate of work done by the material volume $\dot{W}$ is due to the rate of work done by the surface forces $\dot{W_S}$ and the rate of work done by the body forces $\dot{W_b}$. Thus the first law can be written as:

$$\left(\frac{dE}{dt}\right)_{MV} = \dot{Q_V} + \dot{Q_S} - \dot{W_b} - \dot{W_s} \tag{4.13}$$

By definition, work is due to a force acting through a distance and power is the rate at which work is done. Therefore, the rate of work done by body and surface forces can be represented by:

$$\dot{W_b} = -\int_V (\mathbf{f}_b \cdot \mathbf{v})\, dV \tag{4.14}$$

$$\dot{W_S} = -\int_S (\mathbf{f}_S \cdot \mathbf{v})\, dS \tag{4.15}$$

The rate of work due to surface forces can be expanded by replacing $\mathbf{f_S}$ by its

equivalent expression as given in Eq. (4.4) through (4.6). This leads to:

$$\dot{W}_S = -\int_S [\boldsymbol{\sigma} \cdot \mathbf{v}] \cdot \mathbf{n}\, dS = \int_V \nabla \cdot [\boldsymbol{\sigma} \cdot \mathbf{v}]\, dV = -\int_V \nabla \cdot [(-p\mathbf{I} + \boldsymbol{\tau}) \cdot \mathbf{v}]\, dV \tag{4.16}$$

After manipulation, $\hat{W}_S$ can be written as:

$$\dot{W}_S = -\int_V (-\nabla \cdot [p\mathbf{v}] + \nabla \cdot [\boldsymbol{\tau} \cdot \mathbf{v}]\, dV \tag{4.17}$$

If $\dot{q_V}$ represents the rate of heat source or sink within the material volume per unit volume and $\dot{q_S}$ the rate of heat transfer per unit area across the surface area of material element, then $\dot{Q_V}$ and $\dot{Q_S}$ can be written as:

$$\begin{aligned} \dot{Q_V} &= \int_V \dot{q_V}\, dV \\ \dot{Q_S} &= \int_V \nabla \cdot \dot{q_S}\, dV \end{aligned} \tag{4.18}$$

Applying the Reynolds transport theorem and substituting the rate of work and heat terms by their equivalent expressions, Eq.(**??**) becomes:

$$\begin{aligned} \left(\frac{dE}{dt}\right)_{MV} &= \int_V \frac{\partial(\rho e)}{\partial t} + \nabla \cdot [\rho \mathbf{v} e]\, dV \\ &= -\int_V \nabla \cdot \dot{q_S}\, dV + \int_V (-\nabla \cdot [p\mathbf{v}] + \nabla \cdot [\boldsymbol{\tau} \cdot \mathbf{v}]\, dV + \int_V (\mathbf{f_b} \cdot \mathbf{v})\, dV + \int_V \dot{q_V}\, dV \end{aligned} \tag{4.19}$$

Collecting terms together and considering that the integrand has to be zero, the equation is:

$$\frac{\partial(\rho e)}{\partial t} + \nabla \cdot [\rho \mathbf{v} e] = -\nabla \cdot \dot{q_S} + (\nabla \cdot [p\mathbf{v}] + \nabla \cdot [\boldsymbol{\tau} \cdot \mathbf{v}] + (\mathbf{f_b} \cdot \mathbf{v}) + \dot{q_V} \tag{4.20}$$

which represents the mathematical description of energy conservation or simply the energy equation written in terms of specific total energy. The energy equation may also be written in terms of specific internal energy, specific static enthalpy (or simply specific enthalpy), specific total enthalpy, and under special conditions in terms of temperature

## 4.2 Turbolence Modelling

Turbolence in a fluid refers to the three dimensional, unsteady motion of particles that move in a pratically chaotic manner. It appears in the flow field as a

random process that is completely unpredictable. The randomness is present not only in the velocity and pressure functions, but also in the others scalar variables such as temperature and species concentrations that may be present in the fluid [17]. The turbulence problem is of course far from solved, whether in terms of mathematical and intuitive understanding, or in terms of obtaining engineering accuracy for machines that depend on viscous fluid dynamics. Technological fields of global importance such as the airliner and automobile industries revolve around such devices [18].

## 4.3 Standard $k-\epsilon$ Model

This turbulence model involves the resolution of two additional partial differential equations, in order to locally compute the *turbulent eddy viscosity* $\mu_T$ and the *turbulent thermal diffusivity* $\alpha_T$. Like others models based on the *Boussinesq hypothesis*, the $k-\epsilon$ model is based on the following expressions for *turbulent eddy viscosity* $\mu_T$ and for turbulent thermal diffusivity $\alpha_T$:

$$\mu_t = \rho C_\mu \frac{k^2}{\epsilon}$$

$$\alpha_t = c_p \frac{\mu_t}{P_r}$$

where $C_\mu$ is a calibration constant, $k$ is the *turbulent kinetic energy* and $\epsilon$ is the *rate of dissipation of turbulent kinetic energy per unit mass due to viscous stresses.* Solving the following transport equations for $k$ and $\epsilon$ a local value of $\mu_t$ can be computed:

$$\frac{\partial(\rho k)}{\partial t} + \nabla \cdot (\rho \boldsymbol{v} k) = \nabla \cdot ((\mu + \frac{\mu_T}{\sigma_k})\nabla k) + \underbrace{[P_k - \rho\epsilon]}_{S_k}. \tag{4.21}$$

$$\frac{\partial(\rho \epsilon)}{\partial t} + \nabla \cdot (\rho \boldsymbol{v} \epsilon) = \nabla \cdot ((\mu + \frac{\mu_T}{\sigma_k})\nabla \epsilon) + \underbrace{[C_{\epsilon 1}\frac{\epsilon}{k}P_k - C_{\epsilon 2}\rho\frac{\epsilon^2}{k}]}_{S_\epsilon}. \tag{4.22}$$

where $(P_r)$ is the turbulent and the compact form of the production of turbulent energy is given by:

$$P_k = \boldsymbol{\tau}^R : \nabla \boldsymbol{v}$$

It must be kept in mind that the construction of this model is based on two important assumptions:

- *fully turbulent flow*;
- *negligible molecular viscosity effects.*

This establishes the limits of this approach:

- *validity only for high values of the Reynolds*;
- *inability to reach the wall.*

To account for this lack the so-called *low Reynolds* $k$-$\epsilon$ models have also been developed. These models use damping functions to damp the turbulent viscosity while getting close to the wall.

## 4.4 Near the Wall Treatment

On every solid surface, due to the fluid viscosity, a boundary layer develops. This layer of fluid can be divided in three regions:

- *viscous sub-layer* ($0 < y^+ < 5$), where the effect of viscosity dominates;
- *buffer sub-layer* ($5 < y^+ < 30$), where viscous and inertial effects are equal;
- *inertial (log-law) sub layer* ($30 < y^+ < 500$), where the effect of inertia dominates.

These three sub-layers can be identified by the value of $y^+$ that is the dimensionless normal distance ($d_\perp$) from the wall:

$$y^+ = \frac{d_\perp u_\tau}{\nu}, \tag{4.23}$$

where $u_\tau = \sqrt{\tau_\omega / \rho}$ is the velocity scale.

This subdividsion of the boundary layer is schematized in *Figure* 4.1

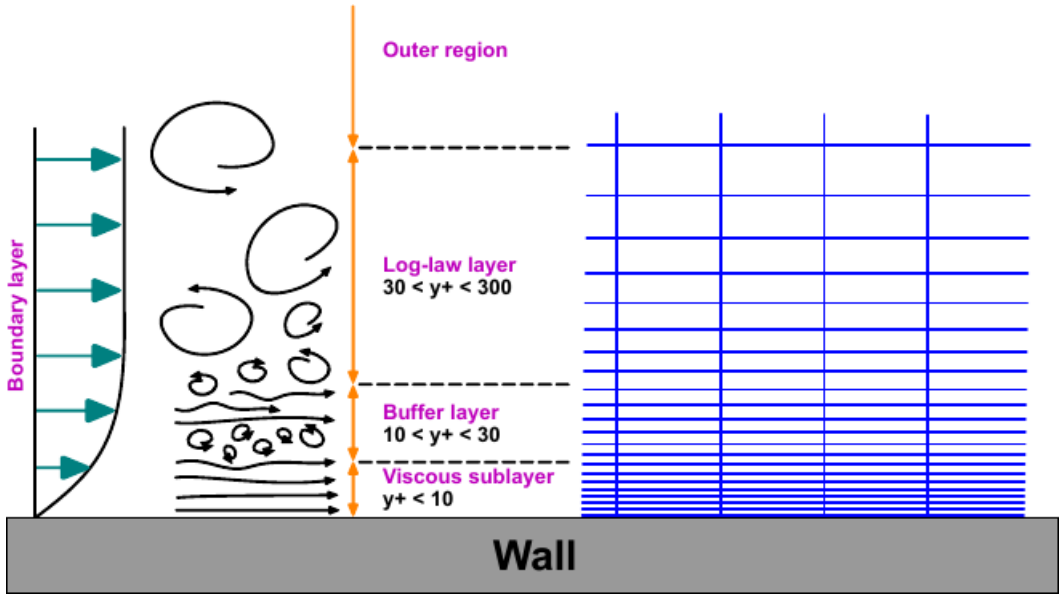


Figure 4.1: *Boundary layer subdivision and correspondent $y^+$ ranges (courtesy of Wolf-Dynamics srl [19])*

.

Turbulence models avoid the *buffer sub-layer*, because the high turbulent production, by placing the first cell center in the *viscous sub-layer* or in the *inertial sub-layer*.

The first option leads to accurate prediction of the boundary layer, but requires a very fine discretization near the wall, usually leading to unaffordable costs.

The second, combined by the definition an appropriate wall-value to each new variable introduced, significantly reduces computational costs while giving a good accuracy. This velocity profile is called *wall function* and its action is schematized in *Figure* 4.2.

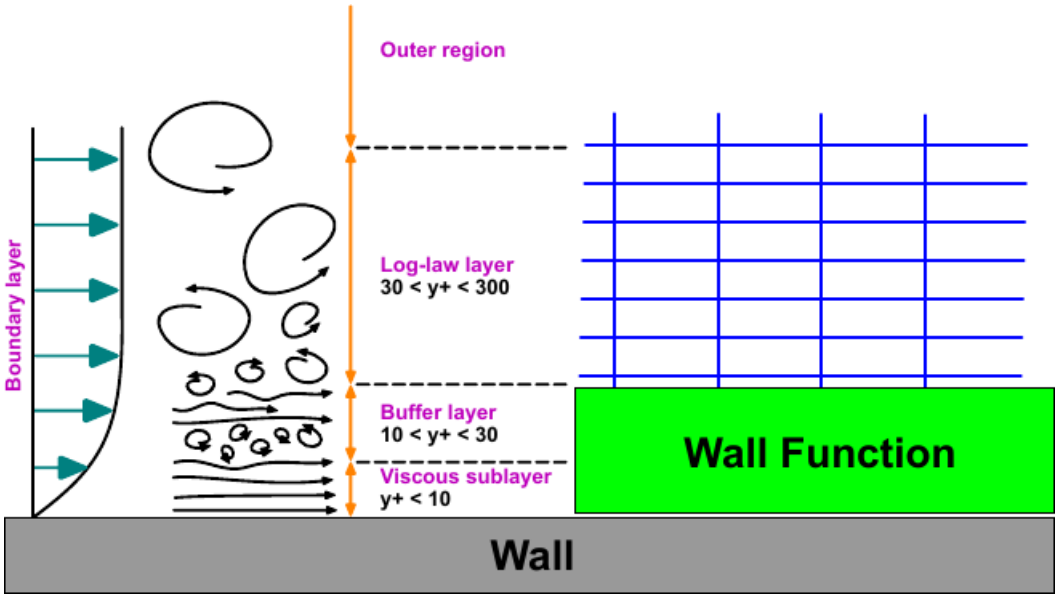


Figure 4.2: *Representation of the wall function approach. (courtesy of Wolf-Dynamics srl [19])*

.

## 4.5 The Finite Volume Method

The Finite Volume Method (FVM) is the standard approach used in most commercial codes for CFD. The equations are solved in a discrete control volume (cell). The typical approach requires to discretize the fluid domain in elementary cells in order to obtain a computational grid (also called mesh), on which to apply iterative resolution methods in order to solve the Navier-Stokes equations or the Euler equations.

In detail, FVM is a numerical technique that transforms the partial differential equations representing conservation laws over differential volumes into discrete algebraic equations over finite volumes (or elements or cells). In a similar fashion to the finite difference or finite element method, the first step in the solution process is the discretization of the geometric domain, which, in the FVM, is discretized into non-overlapping elements or finite volumes. The partial differential equations are then discretized/transformed into algebraic equations by integrating them over each discrete element. The system of algebraic equations is then solved to compute the values of the dependent variable for each of the elements [16].

Discretization of the solution domain produces a computational mesh on which

the governing equations are solved (mesh generation stage). It also determines the positions of points in space and time where the solution will be computed. The procedure can be split into two parts: temporal discretization and spatial discretization. The temporal solution is simply obtained by marching in time from the prescribed initial conditions. For the discretization of time, it is therefore necessary to prescribe the size of the time-step that will be used during the calculation. The spatial discretization of the solution domain of the FVM method presented in this manuscript, requires a subdivision of the continuous domain into a finite number of discrete arbitrary con- trol volume. In our discussion, the control volumes do not overlap, have a positive finite volume and completely fill the computational domain. Finally, all variables are computed at the centroid of the control volumes (collocated arrangement).

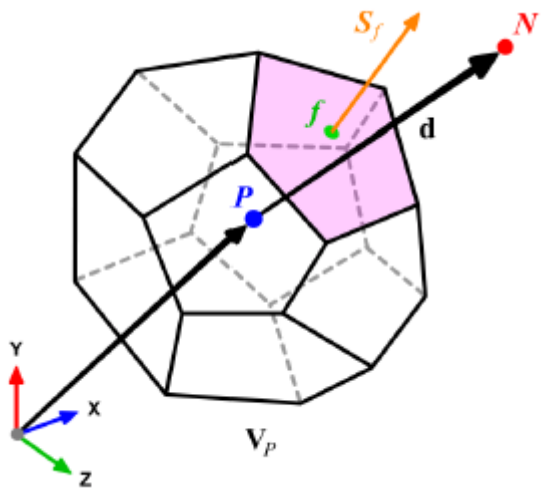


Figure 4.3: *Arbitrary polyhedral control volume $V_P$ . The control volume has a volume V and is constructed around a point P (control volume centroid), therefore the notation VP . The vector from the centroid of the control volume $V_P$ (point P), to the centroid of the neighboring control volume $V_N$ (point N), is defined as* **d**. *The face area vector $S_f$ points outwards from the surface bounding $V_P$ and is normal to the face. The control volume faces are labeled as* ***f****, which also denotes the face center. [20])*

.

A typical control volume is shown in *Figure* 4.3 In this figure, the control volume $V_P$ is bounded by a set of flat faces and each face is shared with only one neighboring control volume. The shape of the control volume is not important for

our discussion, for our purposes it is a general polyhedron. The control volume faces in the discrete domain can be divided into two groups, namely; internal faces (between two control volumes) and boundary faces, which coincide with the boundaries of the domain. The face area vector $S_f$ is constructed for each face in such a way that it points outwards from the control volume, is located at the face centroid, is normal to the face and has a magnitude equal to the area of the face (e.g., the shaded face in *Figure* 4.3). Boundary face area vectors point outwards from the computational domain. In *Figure* 4.3, the point $P$ represents the centroid of the control volume VP and the point N represents the centroid of the neighbor control volume $V_N$. The distance between the point $P$ and the point $N$ is given by the vector $\mathbf{d}$. For simplicity, all faces of the control volume will be marked with $f$, which also denotes the face centroid [20].

For more detailed information about it we recommend the work of J.Guerrero *et al.* [20].

# Chapter 5

# Simulations

The aim of these first simulations is to characterize the field of flux near the face surface, more precisely around the eye surface, that is generated imponing different values of inlet velocity or different turbolence parameters. Moreover we want to point out the primary role of eyelashes influencing the kind of flux and how this varies as the eyelashes length varies. To study the mesh convergence we realized different models that differs between them for the number of cells generated in the three direction x, y, z. The following section will briefly expose the obtained results:

- Mesh Generation
- Grid Convergence

## 5.1 Mesh Geometry

The mesh generation has been carried out basically with two openFOAM utilities: *blockMesh* and *snappyHexMesh* that are controlled respectively by *blockMeshDict* and *blockMeshDict* files. *blockMesh* is a hex structured mesh generator. It allows us to split our geometry into hex blocks, it allows the support of classification of cells sizes even with curved edges. Well suited to simple geometries that can be described by a few blocks, but challenging to apply to cases with a large number of blocks due to book-keeping requirements, i.e. the need to manage point connectivity and ordering.
Once we achieve the subdivision in hex blocks, we can generate the actual mesh

through *SnappyHexMesh*. This is a hex mesh generator that guarantees a minimal level of quality. Controlled using OpenFOAM dictionaries, it is particularly well suited to batch driven operation. Its duty is to generate the actual mesh containing hex and split-hex from the surface geometries. The first step in the meshing process is the cell splitting according to specification defined. Here the user can select several levels and types of refinement for different surfaces, volumes and also edges with the dedicated utility *SurfaceFeatureExtract* [14]. These steps are briefly schemed in the Figure 5.1:

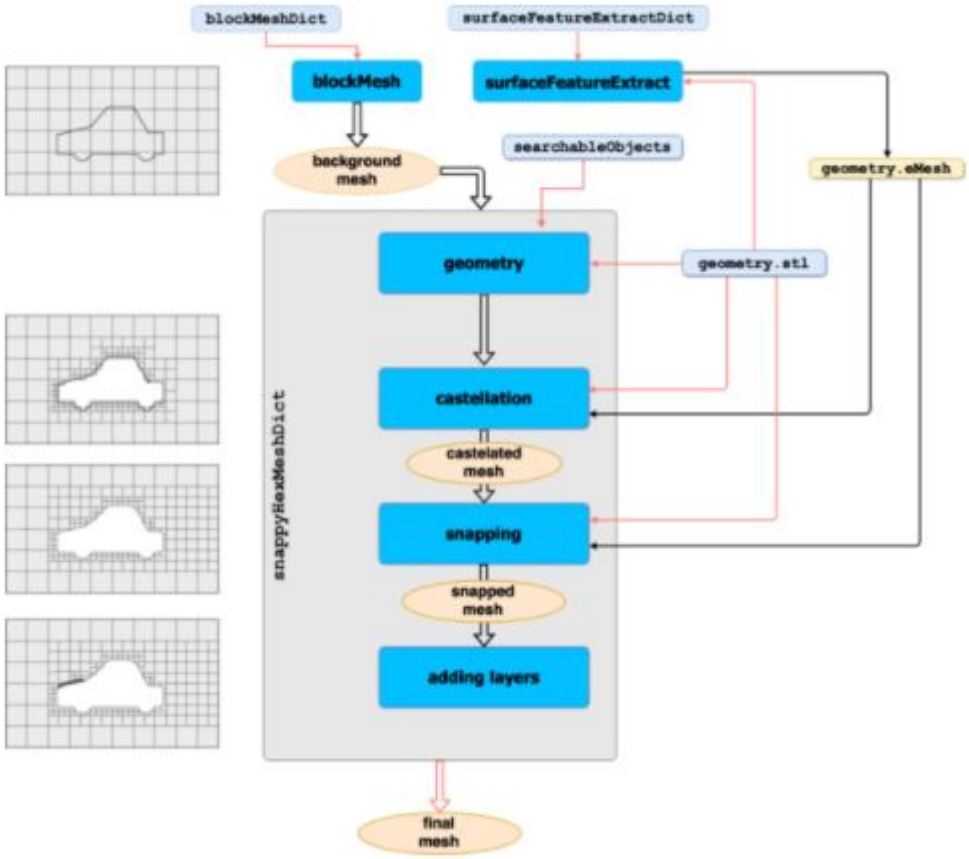


Figure 5.1: *Mesh generation process*

During the process the mesh quality is controlled by the entries in the subdictionary *meshQualityControls*. After the meshing process is completed, the openFOAM utility *checkMesh* will output the feature of the mesh. The most important parameters for checking the quality of the mesh are:

- *Mesh orthogonality*: This parameter is related to angular deviation of the cell

face normal vector from the vector connecting two consecutive cell centres. Non-orthogonality can lead to oscillatory solutions (unboundedness), which in turn can lead to nonphysical values. The higher the non-orthogonal angle (the angle between the face area vector **S** and the vector **d** in *Figure* 5.2 $(a)$), the higher the numerical diffusion, and this in fact reduces the accuracy of the numerical method [20]. Usually this parameter is kept below 75.

- *Mesh skewness*: Skewness is the deviation of the vector that connects two cell centres from the face centres. Skewness can be defined as the deviation of the face centroid $f$ from the point where the vector **d** intercepts the face. This situation is shown in *Figure* 5.2 $(b)$ , where $f$ is the face centroid, $fi$ is the point where the vector **d** intersects the face $f$, and $\Delta_i$ is the vector that represents the deviation of $fi$ from $f$. Skewness adds numerical diffusion to the solution and reduces the accuracy of the numerical method. It also leads to unboundedness, which in turn can conduct to nonphysical results and/or divergence of the solution [20]. Usually this parameter should be kept below 8.

- *Aspect Ratio*: Aspect Ratio $AR$ is the ratio between the longest side $\Delta x$ and the shortest side $\Delta y$ of the cell. Large $AR$ is good if gradients in the largest direction are small.

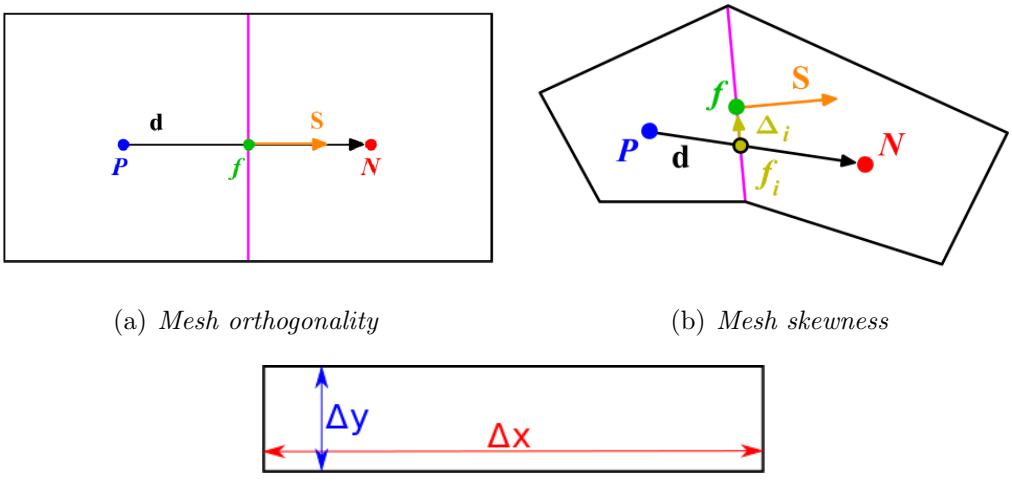


(a) *Mesh orthogonality*

(b) *Mesh skewness*

(c) *Aspect Ratio*

Figure 5.2: *Main mesh quality parameters*

Generally, to produce a mesh it is necessary to take into account two variables: precision and computational effort. The first derives from the degree of accuracy of the mesh: the more refined a mesh is, the closer the simulation will be to reality. The computational effort on the other hand represents the amount of computation necessary to process the mesh: the more accurate a mesh is, the greater the computational effort and, consequently, the time required to process it. In light of these considerations we have chosen to use a fairly refined grid so as not to burden the computational effort too much. Having chosen the study of the defensive behavior of the eyelashes as a field of analysis, it was necessary to produce a finer mesh around the eye and the eyelashes themselves. On the contrary, in the rest of the domain, as will be explained later, our interest was less as there were no significant effects. Below are two images depicting the mesh obtained.

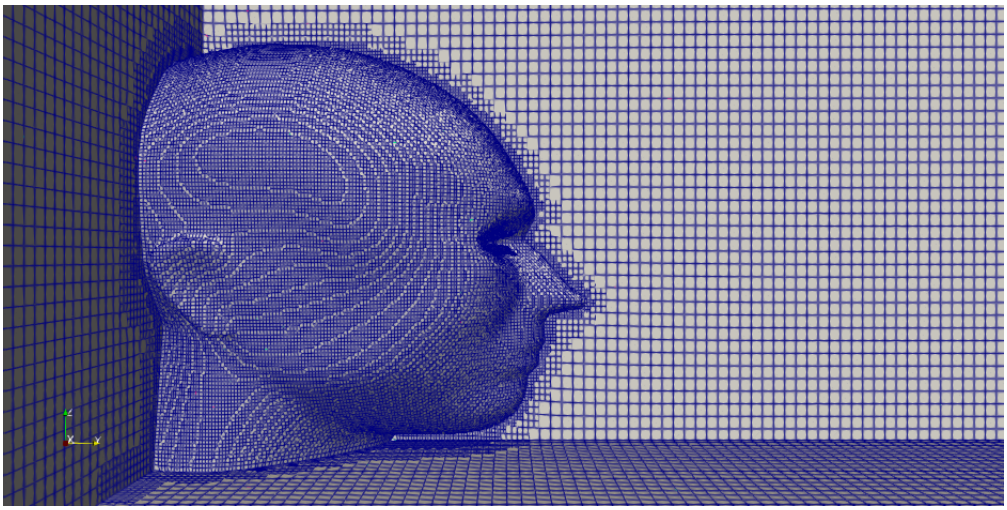

Figure 5.3: *Domain mesh visualization with Paraview*

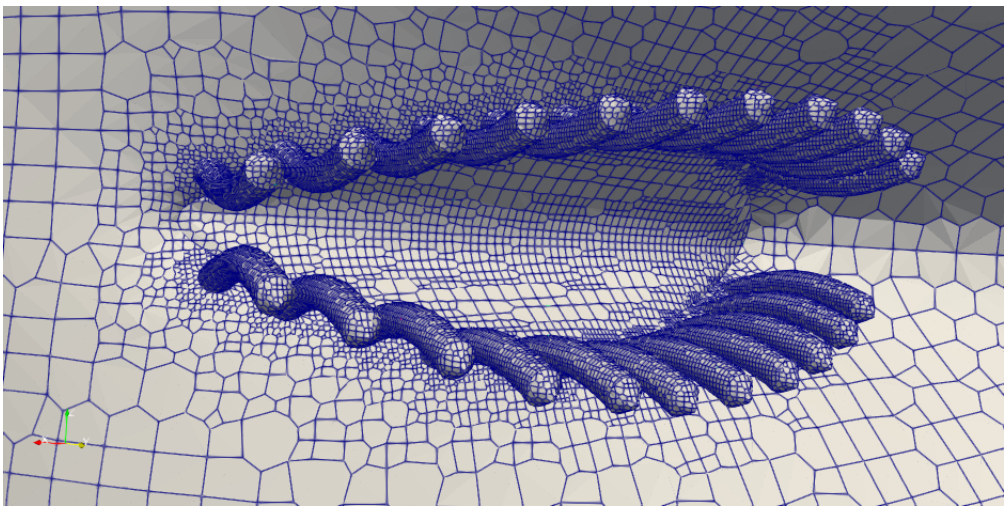

Figure 5.4: *Mesh next to the eyelashes and cornea with paraView*

## 5.2 Grid Convergence

In finite element modeling, a finer mesh typically produces a more accurate solution. However, when a mesh is refined, the time required for processing increases, so a mesh has been obtained that allows us to balance accuracy and processing resources, by performing a mesh convergence study [21]. Following basic steps were required:

- Create a mesh using as few reasonable elements as possible and analyze the model
- Recreate the mesh with a denser element distribution, rerun the analysis and compare the results with those of the previous mesh
- Continue increasing the mesh density and re-analyzing the model until the results converge satisfactorily.

# Part III

# Simulations

# Chapter 6

# Particles Implementations

To numerically model a multiphase flow, it is often important to use separate formulations for the different phases. The *particle phase* consists of bubble, particle, or drops and the *continuous phase* is the fluid in which these particles are generally immersed. The particle can be composed of solid, liquid, or gas, and the continuous fluid can be a liquid or a gas. The coupling between the particle motion and its surroundings can be used to classify the character of the multiphase flow, and thus help determine appropriate numerical techniques. The broadest division is between dispersed and dense flows, and refers to which coupling mechanism primarily determines the particle motion. A multiphase flow can be considered dispersed if the effect of particle-fluid interactions dominates the overall transport of the particles, while it is said to be dense if particle-particle interaction dominates particles motion. Dispersed flows includes one-way coupling (where the dispersed-phase motion is affected by the continuous phase, but not vice versa) and two-way coupling (where the dispersed phase also affects the continuous phase through the interphase coupling). Dense flows usually have four-way coupling where mutual interactions between particles become significant and the effects of the particles on the continuous fluid are weak and often neglected. As well described in [22],volume fraction of particles is the main parameter to make the division between one, two or four way coupling and therefore between dispersed and dense. The volume fraction is defined as $\phi_p = \frac{MV_p}{V}$ where $M$ is the number of particles, $V_p$ is the volume of a single particle and $V$ is the volume occupied by particles and fluid:

- for $\phi_p < 10^{-6}$ there will be one-way coupling;

- for $10{-}6 < \phi_p < 10^{-3}$ there will be two-way coupling and the particles can also increase or dump turbulence;
- for $\phi_p > 10^{-3}$ there will be four-coupling and the flow will be considered as dense.

Another important parameter that may contribute to the selection of the appropriate model is the particle momentum *Stokes number* defined as the ratio between the particle response time $\tau_p$ and that of the system $\tau_s$

$$S_t = \frac{\tau_p}{\tau_s} \tag{6.1}$$

$$\tau_p = \frac{\rho_p d^2}{18\rho_f v} \tag{6.2}$$

$$\tau_s = \frac{L_s}{v_s} \tag{6.3}$$

The equation 6.2 is valid only for *Stokes flow*.

If $S_t \to 0$, the particle behaves as a fluid tracer (momentum one-way coupling) and if $S_t \to \infty$ is unresponsive to the ow variations. One would define a Stokes number not only for momentum but also for mass and temperature in order to evaluate with more precision the mass coupling and energy coupling of particles with the continuous phase. If two-way coupling is considered, it simply involves some source terms in the continuous phase equations (momentum, energy, turbulence models...) that are generally described in an Eulerian reference frame. For the sake of simplicity, we have limited our interest to the one-way coupling.

### 6.0.1 Particle equations

Various treatments of the particle field can be employed. Particles could be described in an Eulerian or Lagrangian reference frame and, as suggested by *E. Loth* in his paper [23], distinctions could be done about the treatment of particle surface forces. In this work only the Lagrangian approach will be discussed. With this reference frame the particles are treated as individual and properties are updated along the path of each particle. For the treatment of the surface forces, the point- force treatment represents the ow over the particle with empirical and theoretical treatments (specifying a drag or lift coefficient) to obtain the force on the particle. For the resolved surface treatment, the fluid dynamics (e.g.,

pressure and shear stress distributions) are fully resolved over the entire particle surface and then integrated to obtain the overall hydrodynamic forces. Following the point-surface approach and defining $\boldsymbol{x_p}$ as the particle centroid and $m_p$ the particle mass, Lagrangian particle equation of motion is:

$$m_p \frac{\partial \boldsymbol{v}}{\partial t} = \boldsymbol{F_{body}} + \boldsymbol{F_{surf}} \tag{6.4}$$

The left hand side represents the particle mass inertia and the right hand side represents the sum of body forces and surface forces on the particle. Body forces are those related to gravitational effects:

$$\boldsymbol{F_{body}} = \frac{(\rho_p - \rho)\pi d_p^3}{6}\mathbf{g} \tag{6.5}$$

where $d_p$ and $\rho_p$ are respectively the droplet diameter and droplet density. Surface forces can be seen as the sum of different terms: drag, virtual mass, a term related to pressure gradient and one to the "history" of particle (Basset term). The expressions for all these terms are listed below without a rigorous derivation:

The drug force is:

$$F_{d,i} = \frac{1}{2}\frac{\pi d_p^2}{4}\rho_f C_d \mid \boldsymbol{u}\text{-}\boldsymbol{u_p} \mid (u\text{-}u_{p,i}) \tag{6.6}$$

with

$$C_d = \frac{24}{Re_p}(1 + \frac{3}{16}Re_p)$$

The pressure gradient force is:

$$F_{p,i} = \frac{1}{6}\pi d_p^3 \rho_f \frac{Du_i}{Dt} \tag{6.7}$$

The added mass force (virtual force) is:

$$F_{A,i} = \frac{\pi d_p^3}{12}\rho_f \left(\frac{Du_i}{Dt} - \frac{\partial u_{p,i}}{\partial t}\right) \tag{6.8}$$

The Basset force is:

$$F_{B,i} = \frac{3}{2}d2_p\rho_f\sqrt{\pi\nu}\int_\infty^t \frac{\partial}{\partial\tau}(u_i - u_{i,p})\frac{\partial\tau}{\sqrt{t-\tau}} \tag{6.9}$$

where $Re_p$ is the particle Reynolds number based on relative velocity:

$$Re_p = \frac{\rho d_p(\boldsymbol{u}\ \text{-}\boldsymbol{u_p})}{\mu} \tag{6.10}$$

where $\rho$ is the density of the continuous phase. A better description of all these terms can be found in [23] and [24].

## 6.1 Dispersion Models

Dispersion models are methods that seek to predict how turbulence affects the particles motion. They are employed for RANS (*Reynolds Averaged Navier Stokes equations*) simulations with particles in order to account the effect of unresolved turbulent structures. For this reason it is clear that these models will not be used on LES (*Large Eddy Simulation*) or DNS (*Direct Numerical Simulation* simulations because the turbulent structures will be filtered and solved or completely solved. The idea behind those methods is to allow particle simulations without the need of a LES or DNS solutions which are extremely time consuming. On the other side these models will have less accuracy and an extremely complex mathematics involving stochastic variables in partial differential equations. In openFOAM two dispersion models are implemented: *Stochastic Dispersion Model* and *Gradient Dispersion Model*. The *Stochastic Dispersion Model* adds a stochastic component $\boldsymbol{u_{turb}}$ at the fluid velocity $\boldsymbol{u}$ that is seen by each particle. The velocity associated with particles $\boldsymbol{u_p}$ that determines the forces previously described is computed as it follows:

$$\boldsymbol{u}_p = \boldsymbol{u} + \boldsymbol{u_{turb}} \tag{6.11}$$

The magnitude of $\boldsymbol{u_{turb}}$ is chosen for each parcel from a Gaussian random number distribution with standard deviation related with the turbulent kinetic energy $k$.

# Chapter 7

# Results

## 7.1 Flux Generation

All simulations were carried out using the OpenFOAM software. The solver used in all four cases of generating the flow field is *simpleFoam*, a steady-state solver for incompressible, turbulent flow. The solver settings in the files *fvSolution fvSchemes* have been kept constant. Each simulation can be interrupted before the pre-established final time, in case the parameters have already reached convergence. Post-processing continues through the use of Paraview software. In this way we are able to graphically display the results obtained in relation to four different parameters: $U$ (velocity), $p$ (pressure), $k$ (turbulent kinetic energy) and $\epsilon$ (rate of dissipation of turbulent kinetic energy). Each of these variables can be visualized on the three planes $x, y, z$. The obtained representations allow to formulate various considerations of a physical nature.
In the next section we will report the results and the relative interpretations extrapolated from them.

### 7.1.1 Results

The analysis of the results starts with the setup that has an input speed of 3.5 $m/s$. The flow that we have generated within our domain is uniform. The two most important parameters that characterize the flow are the velocity and the pressure. These two parameters assure values almost constant throughout the domain. Their variation occurs close to the face, where the flow field is actually perturbed. We can find this behavior for all four cases analyzed, as can be seen

in the figures below, which show a slice of the orthogonal domain respectively at the $Y$ axis (*Figures* 7.1), and at the $Z$ axis (*Figures* 7.2):

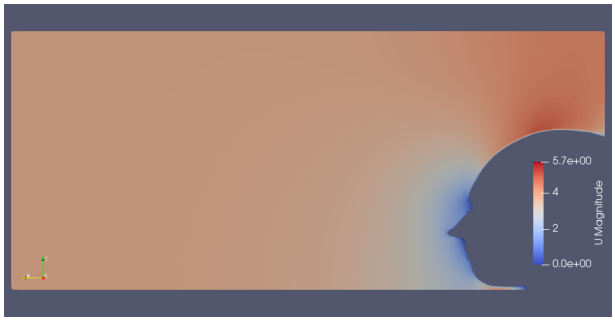


(a) *Without eyelashes*

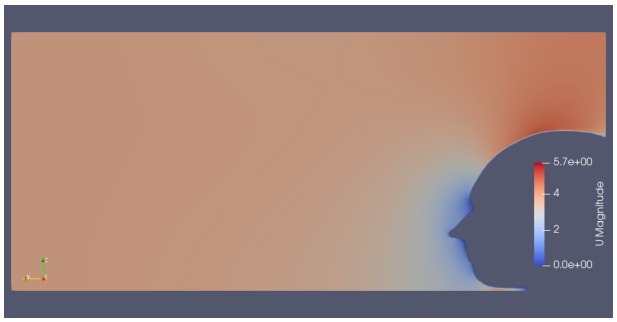


(b) *3.3mm eyelashes*

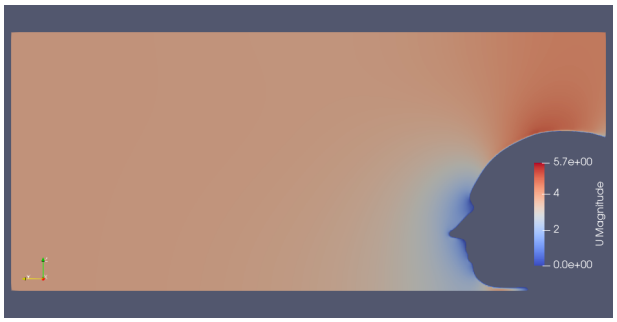


(c) *6.6mm eyelashes*

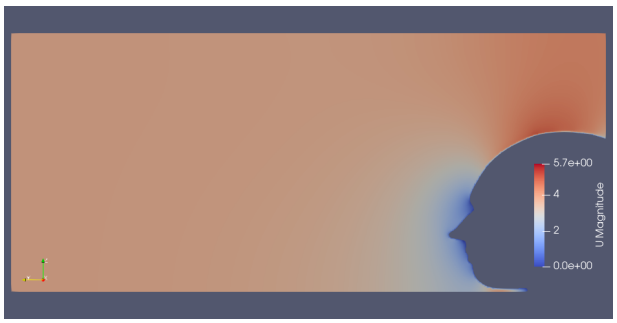


(d) *1cm eyelashes*

Figure 7.1: *Slice depicting the velocity magnitude along the West plane for the four cases analyzed*

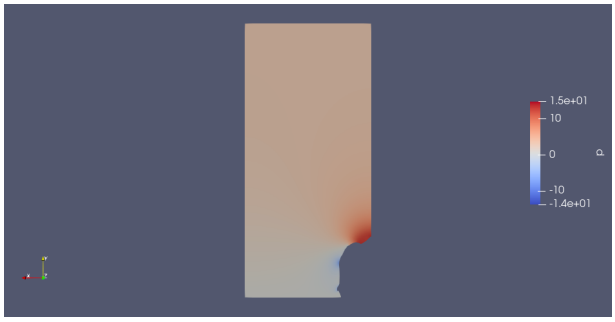


(a) *Without eyelashes*


(b) *3.3mm eyelashes*


(c) *6.6mm eyelashes*


(d) *1cm eyelashes*

Figure 7.2: *Slice normal to the Z axis depicting the progress of the Pressure for all four cases*

From these images we can distinctly notice how the pressure is large when the speed is small: in fact, around the face the values of the velocity decrease to zero while those of the pressure increase. In particular, it can be better understood from *Figures* 7.3, 7.4 how it is the nose that channels the flow and directs it in the direction of the eye. This aspect will be commented in connection with the deposition of the particles. In general, a fundamental aspect of this work is to establish how the velocity field vary as the eyelash length varies, since this will affect the movement and adhesion of solid particles on the eye. To better understand this aspect, we considered the trend of the current lines of the velocity module and pressure for each case. The results are shown in the *Figures* 7.3 and 7.4:

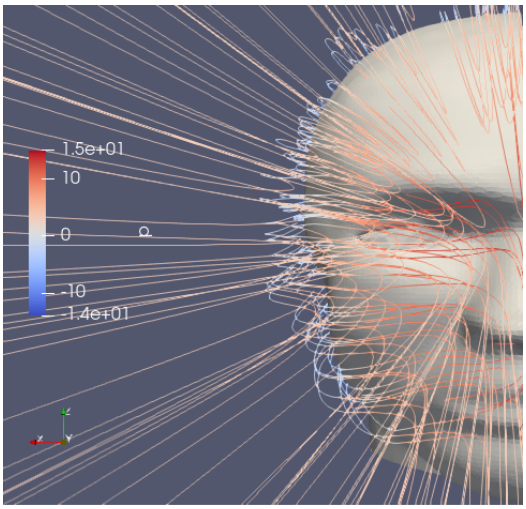


(a) *Without eyelashes*

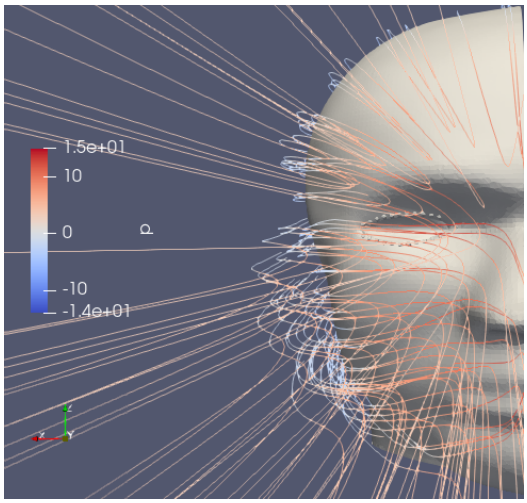


(b) *3.3mm eyelashes*

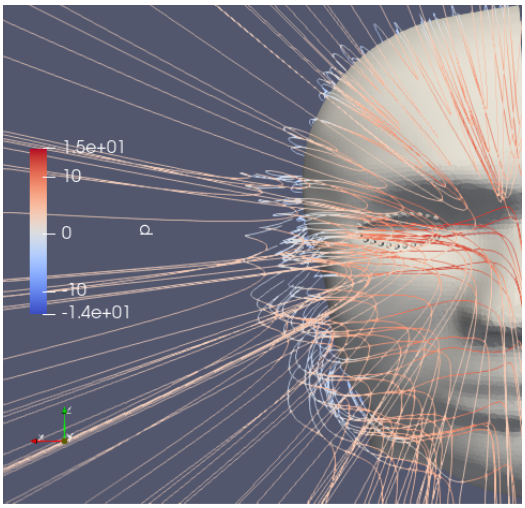


(c) *6.6mm eyelashes*

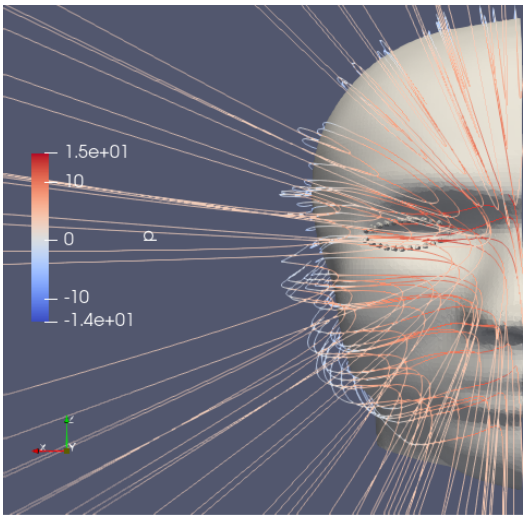


(d) *1cm eyelashes*

Figure 7.3: *Current lines depicting the pressure trend display via Paraview software*

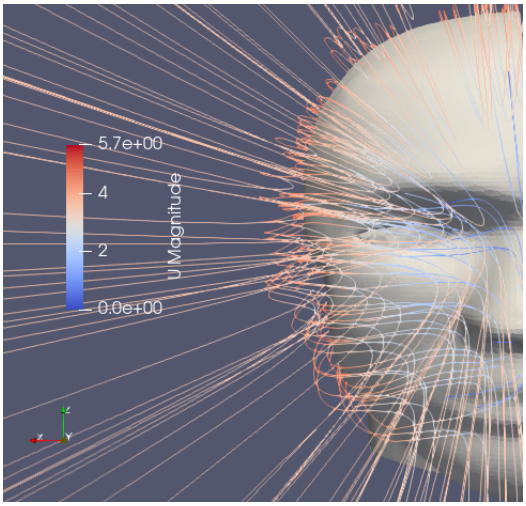


(a) *Without eyelashes*

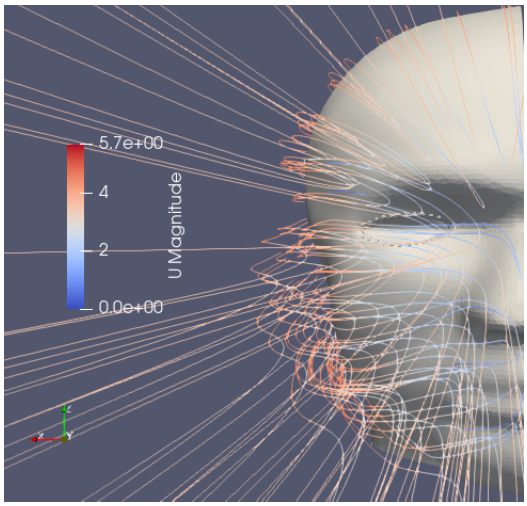


(b) *3.3mm eyelashes*

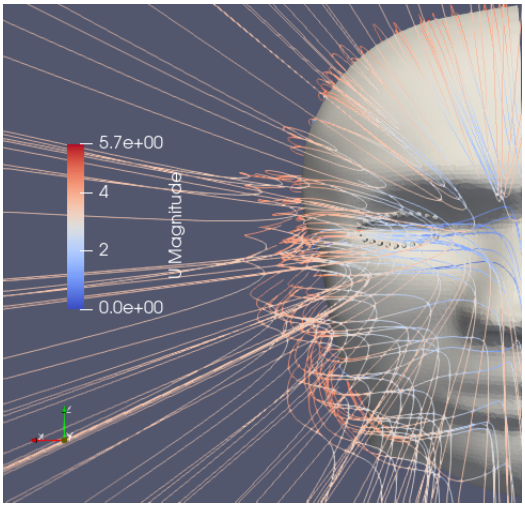


(c) *6.6mm eyelashes*

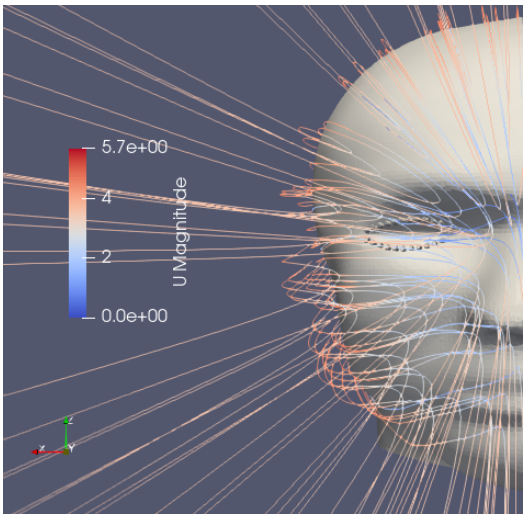


(d) *1cm eyelashes*

Figure 7.4: *Current lines depicting the velocity trend display via Paraview software*

From these images it is easier to understand what was previously said both as regards the connection that is created between pressure and the velocity module, and as regards the function of the various anatomical elements such as the nose in channeling the field of flow.

## 7.2 Particles Deposition

All simulations were carried out using the OpenFOAM software. The solver used in all four cases of particle stream generation is *icoUncoupledKinematic-ParcelFoam*, which is an unsteady solver for Lagrangian particle clouds. Having understood how the flow field is generated and how its parameters vary, it is now crucial to understand specifically how eyelashes influence the flow field around the eye. The set up and choice of the first case, whose values have been entered in the directory *kinematicCloudProperties*, has been chosen as follows for each particle:

- Diameter: variable with normal distribution $\mu$m
- Density $\rho$: 1000 $kg/m^3$

In this case, the distribution of the particles was assigned as *Normal*, and in this way it was assumed that the particles had different diameters; although moving away from a real case in which the distribution could not be evaluated as normal, this distribution is effective as a preliminary study. The choice of this distribution, follows the work of Xie et al. [25] in which the size of the particles was evaluated between 60 and 100 $\mu$m.
In the second and third cases we have chosen fixed values for the diameter of the particles. In particular, for the second case we have:

- Diameter: 100 $\mu$m
- Density $\rho$: 1000 $kg/m^3$

While for the third case we chose the following parameters:

- Diameter: 50 $\mu$m
- Density $\rho$: 1000 $kg/m^3$

During the dynamic, the particles are subjected to the effect of the motion field and can interact with the surfaces of the computation volume in a different way: get stuck (type stick), rebound on them (type rebound) or cross them (type escape). The various surfaces have been set up as follows:

- Top: type Rebound

- Face: type Stick
- Cornea: type Stick
- Ciglia: type Stick
- Bottom: type Escape
- North, South, East, West: type Escape

It is known that the computational effort in particles simulations is strickly related with the total number of particles. For this reason the choice moved on the case with the lowest number of particles; the total number of particles per second that was chosen is $n_{particles/second} = 5000$. Often it's not possible to simulate the real number of particles because this value can easily be equal to milions or bilions and it is closely connected to the situation and the environment. Despite this, a strong point of the discussion is the choice, as we will see in the next paragraph, to study the normalized process of distribution of the particles on the various patches. For this reason the subjects of the study are the derivatives relative to the time of each distribution. Therefore the choice of the number of particles per second becomes strategic not only to make the treatment statistically valid, but also to lighten the weight of the calculations. This is granted to us since we do not take into account the collisions between particles and the force of the particles on the flow itself.

### 7.2.1 Results

To ensure a logical coherence to the work, even the incoming particles have been assigned a speed of 3.5 $m/s$. Having understood how the flow field is generated and how its parameters vary, it is now crucial to understand specifically how the eyelashes influence the generation of the flow field around the eye. *Figures* 7.5, 7.6, 7.7, 7.8 represents an orthogonal section to the $Y$ axis of the flow field generation speed at the final instant of our simulation. We have generated this section in such a way that it intersects the eyelashes to verify their role and impact as their length varies.

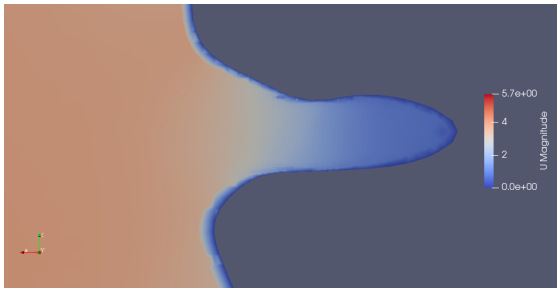


(a) *U magnitude*

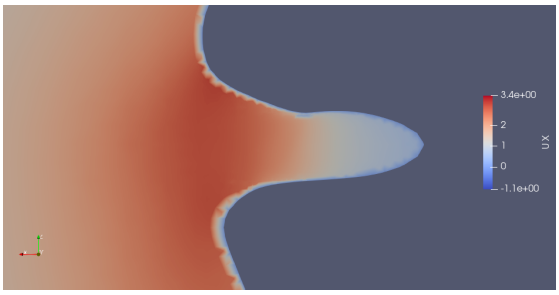


(b) *Ux*

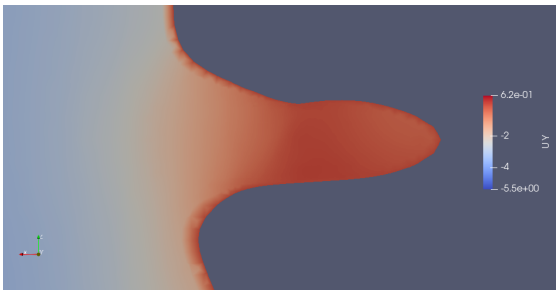


(c) *Uy*


(d) *Uz*

Figure 7.5: *Slice normal to the Y axis depicting the trend of the velocity magnitude and the velocity along the three directions x, y, z for the case without eyelashes*

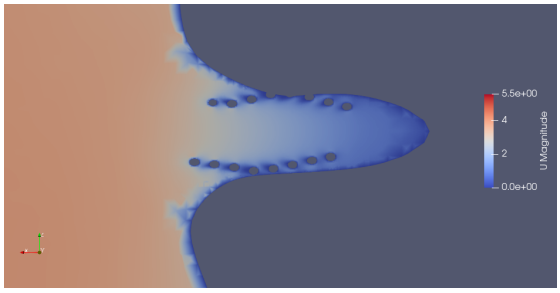


(a) *U magnitude*

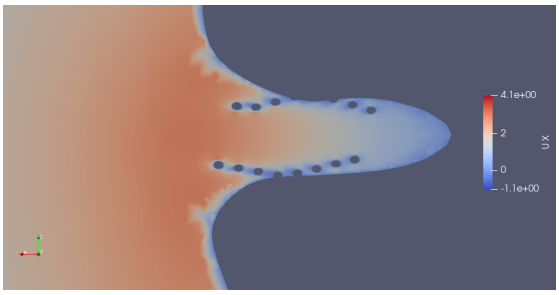


(b) *Ux*

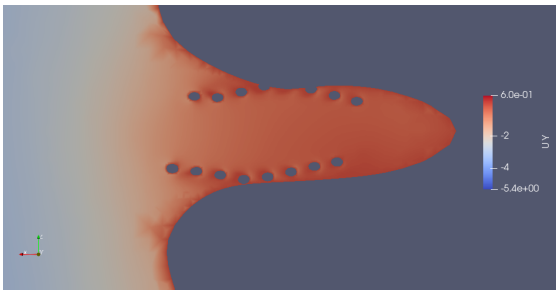


(c) *Uy*

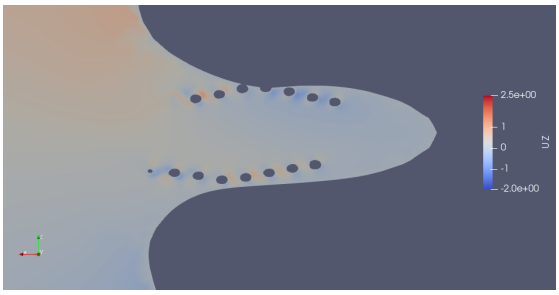


(d) *Uz*

Figure 7.6: *Slice normal to the Y axis depicting the trend of the velocity magnitude and the velocity along the three directions x, y, z for the case with 3.3mm long eyelashes*

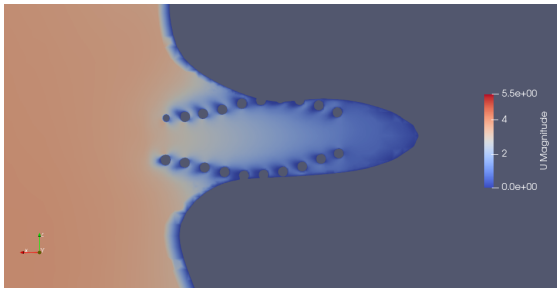


(a) *U magnitude*

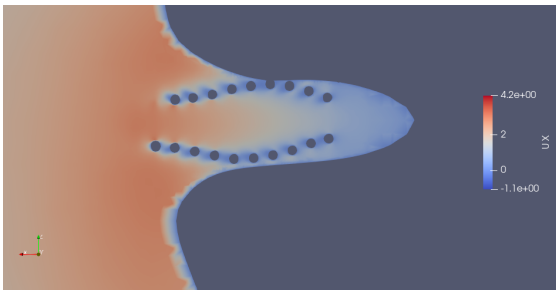


(b) *Ux*

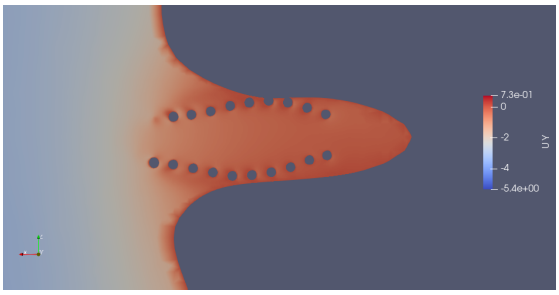


(c) *Uy*

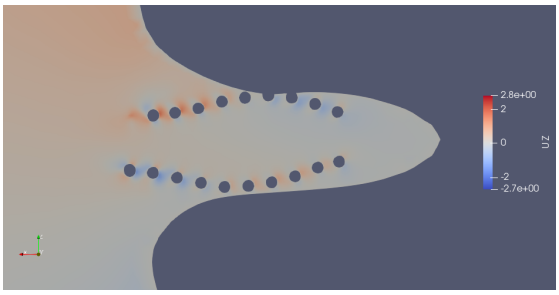


(d) *Uz*

Figure 7.7: *Slice normal to the Y axis depicting the trend of the velocity magnitude and the velocity along the three directions x, y, z for the case with 6.6mm long eyelashes*

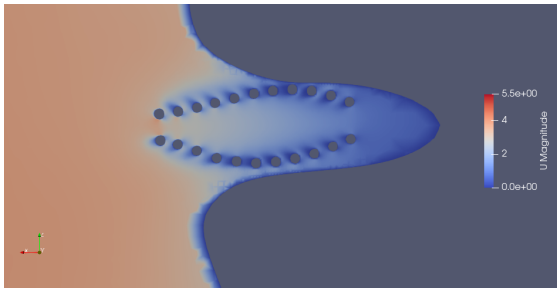


(a) *U magnitude*

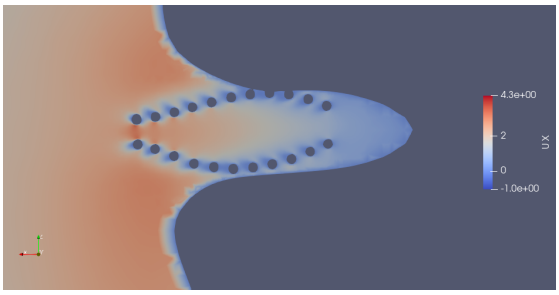


(b) *Ux*

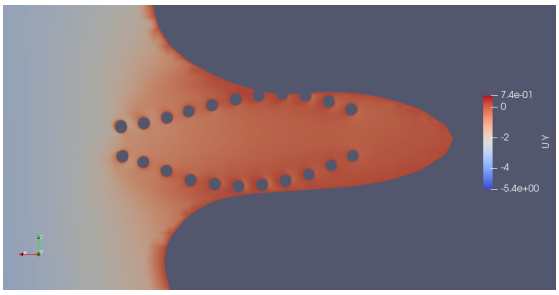


(c) *Uy*

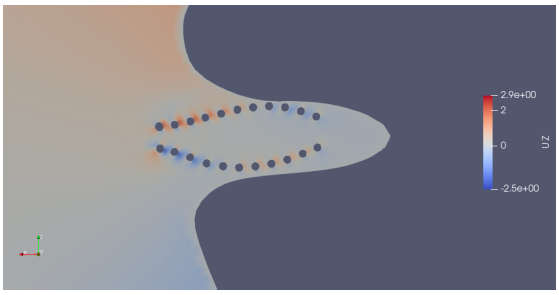


(d) *Uz*

Figure 7.8: *Slice normal to the Y axis depicting the trend of the velocity magnitude and the velocity along the three directions x, y, z for the case with 1cm long eyelashes*

As can be seen from the previous figures, the eyelashes influence the flow field. Specifically, we thought an in-depth analysis of the speed parameter was particularly relevant in the discussion. As can be seen, the velocity field is strongly influenced by the presence of the cilia as regards the space immediately near the ocular surface. The difference in the generation of the velocity field can be found in each of the three directions of space:

- Along the X axis the eyelashes have a strong influence on the generation of speed from the flow field. In particular, in the case without eyelashes, we find an increase in speed as we move away from the nose in the direction of the ear. This increase is instead damped in the case with the eyelashes: these contribute to forming an increase of speed in the junction between upper and lower eyelashes on the temporal side. We also observe how the speed suddenly decreases around the eyelashes themselves, reaching almost 0.

- Along the Y axis the velocity field without eyelashes increases as you approach the nose. The eyelashes in this case contribute to a variation of the velocity field especially in the space between each of them. In fact, right here we find an accumulation of speed.

- Along the Z axis, the flow field appears less intense and it decreases as it approaches the nose. The effect of the eyelashes in this case appears particularly evident. The flow is modified differently in each of the four regions into which we can divide the eye: in the upper region closest to the ear the velocity field undergoes an increase between one eyelash and another and a decrease in the area immediately anterior and posterior of the eyelashes; similarly, but with less intensity, it occurs in the lower region closest to the nose. In the lower region near the ear, the prevailing effect is the decrease in the flow velocity field between one eyelash and another; similarly but with less intensity in the upper region near the nose.

Based on the considerations analyzed so far, let's study the first case, the one characterized by the normal distribution of the particle diameter. The first thing we considered important to evaluate was the tendency of the particles to attach themselves to the domain. The phenomenon of increased interception tendency of eyelashes as their length increases is proportional to the decrease of this tendency

of the cornea which, progressively, is increasingly protected by longer eyelashes. This process has been studied in depth: as can be seen from the *Figures* 7.10 and 7.11, the growth or decrease trend of the number of particles stuck to the different surfaces can be simplified with a linear trend. The red line in the face, eyelash and cornea graphs is the most faithful approximation of our data cluster with a straight line.

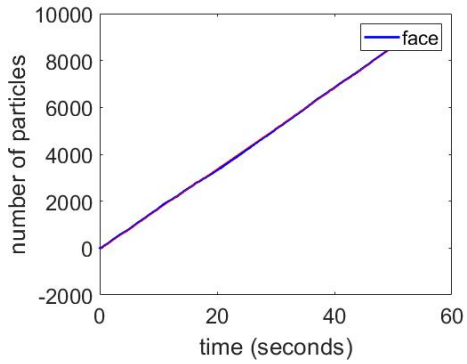


(a) *Case without eyelashes*

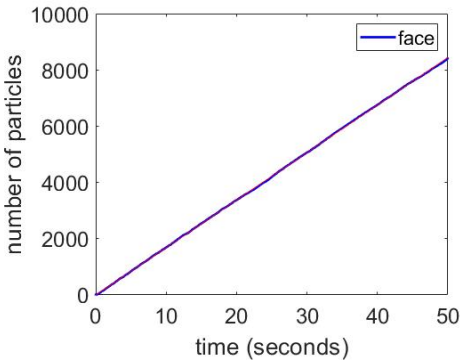


(b) *Case eyelashes 3.3mm*

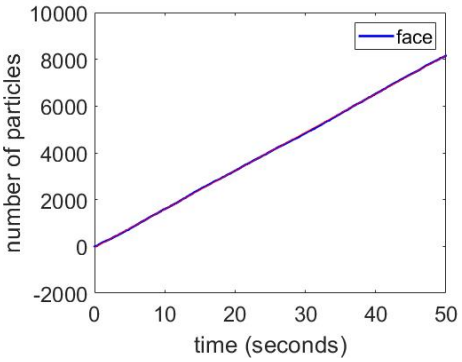


(c) *Case eyelashes 6.6mm*

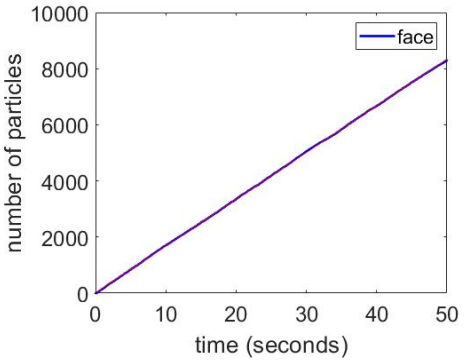


(d) *Case eyelashes 1cm*

Figure 7.9: *Deposition of parcels with variable diameter on the face*

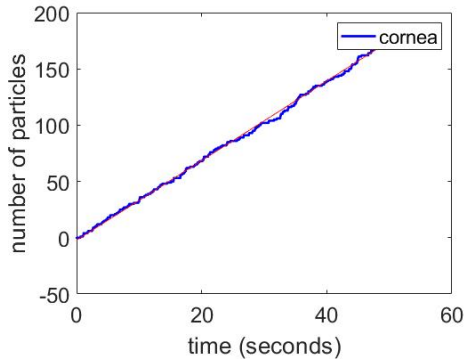


(a) *Case without eyelashes*

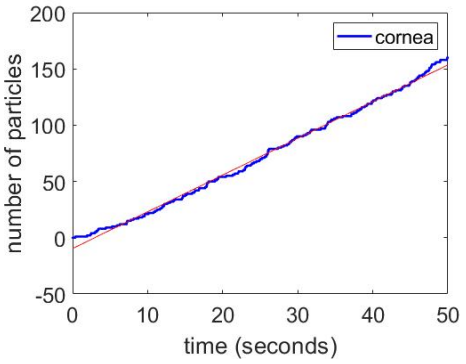


(b) *Case eyelashes 3.3mm*

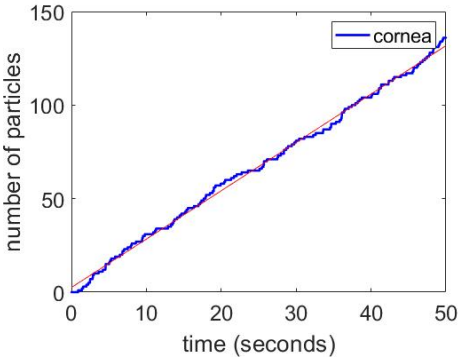


(c) *Case eyelashes 6.6mm*

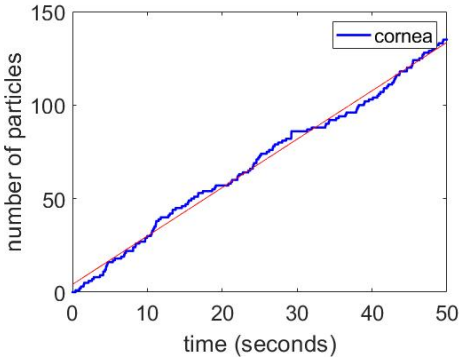


(d) *Case eyelashes 1cm*

Figure 7.10: *Deposition of parcels with variable diameter on the cornea*

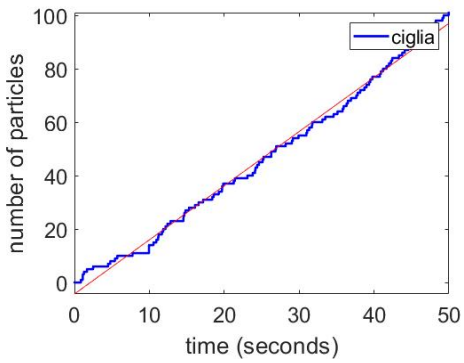


(a) *Case eyelashes 3.3mm*

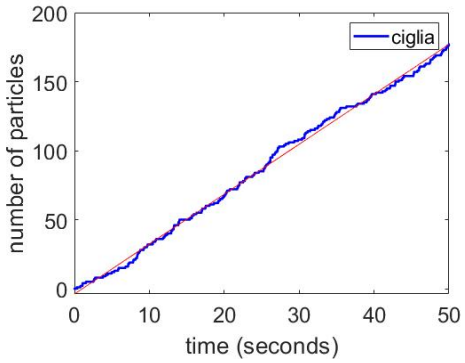


(b) *Case eyelashes 6.6mm*

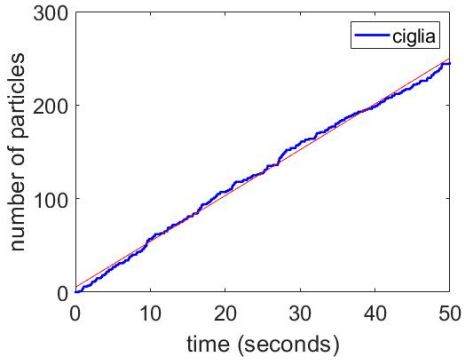


(c) *Case eyelashes 1cm*

Figure 7.11: *Deposition of parcels with variable diameter on the eyelashes*

The results just obtained have been studied as it was decided to analyze how the slope of these lines changed. In other words we have calculated the first derivative. As shown numerically in *Table* 7.1, and graphically in *Figure* 7.12, the values obtained appear consistent: as the length increases, the eyelashes trap more and more particles, unlike the face but above all the cornea which reduce their range of action.

| | $\frac{dNumberofParcels}{dt}$ | | | |
|---|---|---|---|---|
| | ***case 0*** | ***case 3.3mm*** | ***case 6.6mm*** | ***case 1cm*** |
| Face | 172.4 | 169 | 164.2 | 166.5 |
| Cornea | 3.536 | 3.263 | 2.585 | 2.588 |
| Ciglia | / | 2.026 | 3.617 | 4.901 |

Table 7.1: *Relationship between the derivative of the number of particles, considered with variable diameter according to a normal distribution, with respect to time and the length of the eyelashes for the three patches: face, cornea and eyelashes*

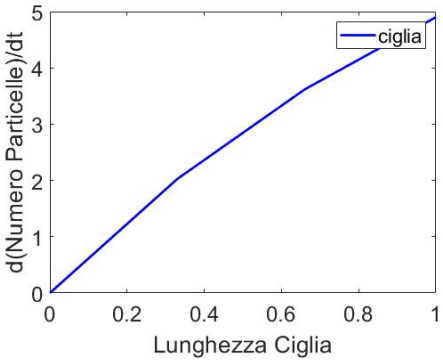


(a) *Eyelashes Patch*

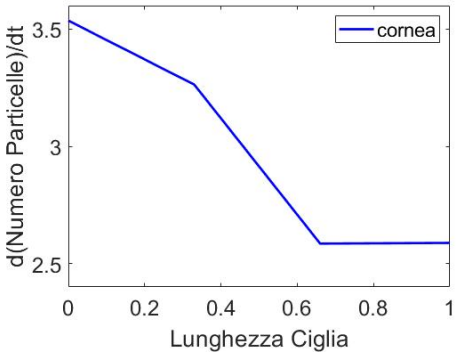


(b) *Cornea Patch*

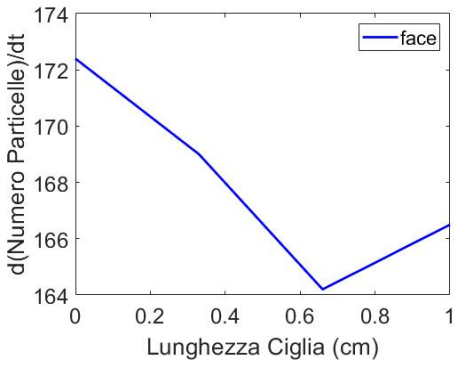


(c) *Face Patch*

Figure 7.12: *Graphical results to Table 7.1*

For all four case studies, the trend of particles entering the domain and sticking with respect to the total number of particles appears to be consistent. The only exception is the face which, however, represents a broader statistical phenomenon as it is not actually protected by the eyelashes.
A second part of the analysis focused on a qualitative assessment of the deposition of the particles on the surfaces of the cornea and eyelashes: as we can see in the *Figure* 7.13, the depositions in all four cases appear homogeneous, without agglomerations in certain points of the geometry.

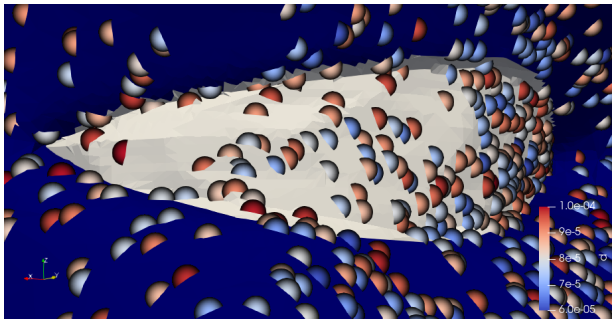


(a) *Case without eyelashes*

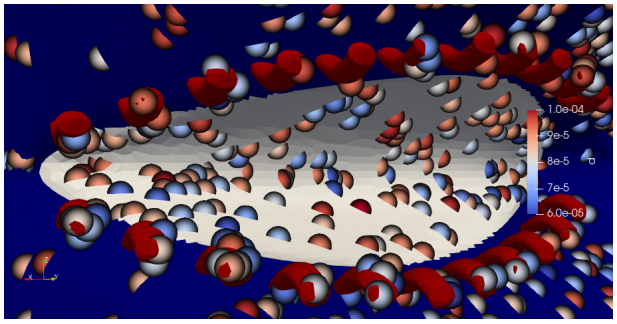


(b) *Case eyelashes 3.3mm*

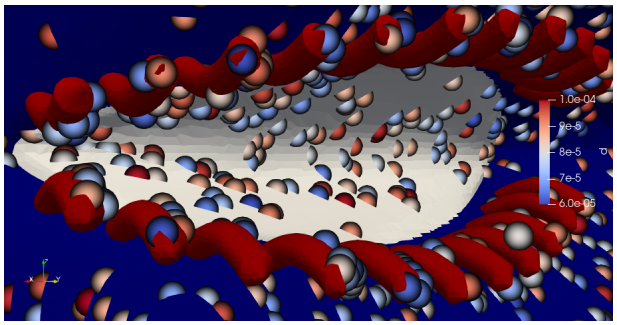


(c) *Case eyelashes 6.6mm*

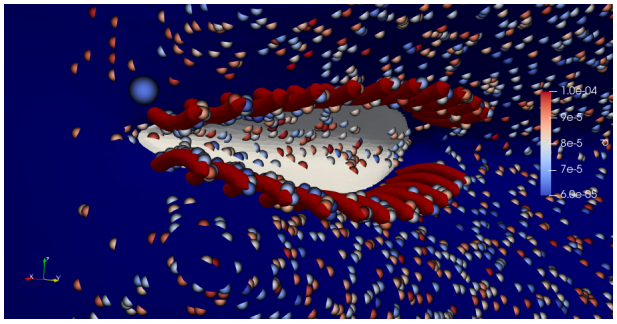


(d) *Case eyelashes 1cm*

Figure 7.13: *Parcels deposition*

Even only through the visual qualitative investigation it is possible to understand how the length parameter is crucial in the discourse relating to the deposition of particles. In fact, by comparing the various simulations we can formulate some hypotheses. First it is verified that the flow field generated in the cases with eyelashes differs from the case without eyelashes. We find this difference by analyzing the deposit areas of the particles. By restricting the analysis around the ocular area, it seems that the particles adhere better in areas where the flow velocity range is smaller. The role of the eyelashes in this context was twofold: in addition to protecting the ocular surface, it helped to produce a homogeneous flow field around the ocular surface characterized by damped values compared to the case without eyelashes.
Having analyzed the first case, our analysis continues with the second and third cases, those characterized by particles with a fixed diameter. To study these two situations we thought it was interesting to compare the results obtained, to verify if and how the adhesion process of particles could change. Observing the results obtained from these simulations we noticed that the adhesion trends were almost linear. For this reason it was thought, as in the first case, to approximate these behaviors with straight lines in order to be able to calculate the first derivative in a simple way. The results of this analysis are shown in the two *Tables* 7.2 and 7.3:

| | $\frac{dNumberofParcels}{dt}$ | | | |
|---|---|---|---|---|
| | ***case 0*** | ***case 3.3mm*** | ***case 6.6mm*** | ***case 1cm*** |
| Face | 55.94 | 53.51 | 51.7 | 51.18 |
| Cornea | 0.702 | 0.501 | 0.418 | 0.495 |
| Ciglia | / | 1.519 | 3.271 | 4.720 |

Table 7.2: *Relationship between the derivative of the number of particles, considered to be of a constant diameter (50* $10^{-}6$ $\mu m$*), with respect to time and the length of the eyelashes for the three patches: face, cornea and eyelashes*

| | $\frac{dNumberofParcels}{dt}$ | | | |
|---|---|---|---|---|
| | ***case 0*** | ***case 3.3mm*** | ***case 6.6mm*** | ***case 1cm*** |
| Face | 267.6 | 261.6 | 259.5 | 257.6 |
| Cornea | 5.198 | 5.022 | 4.880 | 4.112 |
| Ciglia | / | 1.963 | 3.152 | 3.959 |

Table 7.3: *Relationship between the derivative of the number of particles, considered to be of a constant diameter (100* $10^{-}6$ $\mu m$*), with respect to time and the length of the eyelashes for the three patches: face, cornea and eyelashes*

By changing the size of the particles we also change their inertia and, consequently, their ability to get close to the surface of interest and then adhere to it. We have decided to report the values shown in the tables graphically, as shown in the *Figures* 7.14 and 7.15:

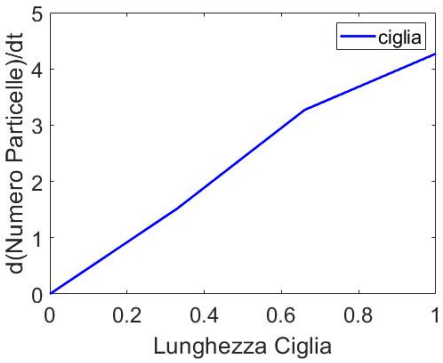


(a) *Eyelashes Patch*

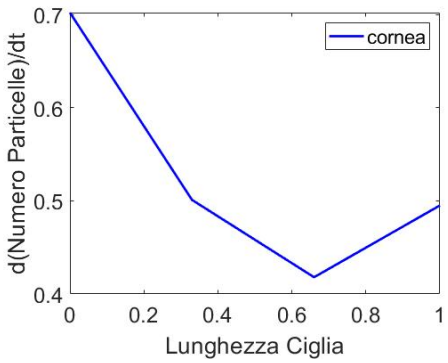


(b) *Cornea Patch*

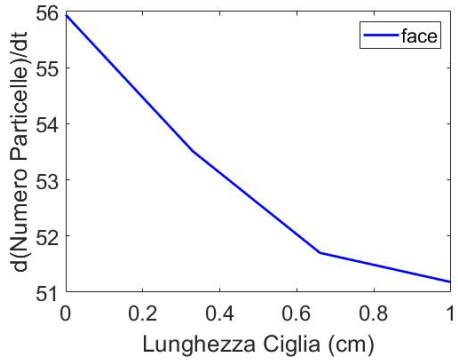


(c) *Face Patch*

Figure 7.14: *Graphical results to Table 7.2*

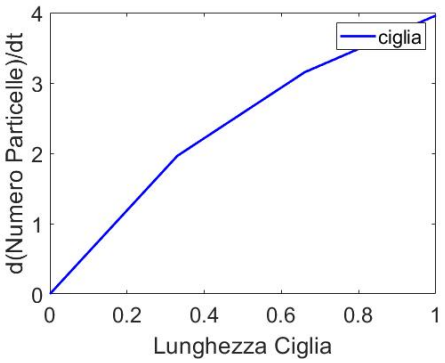


(a) *Eyelashes Patch*

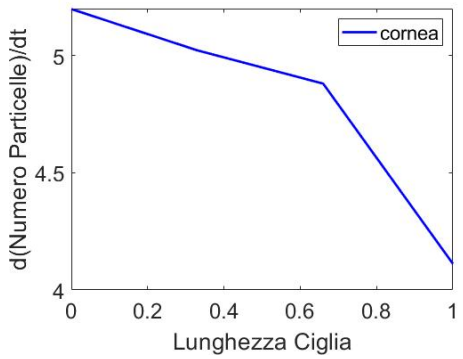


(b) *Cornea Patch*

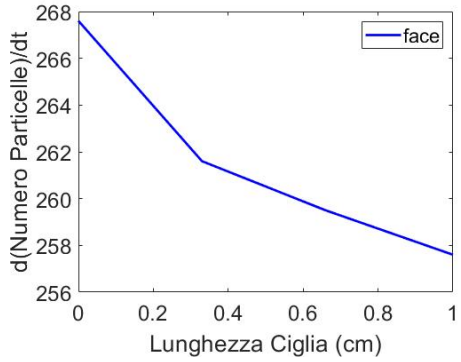


(c) *Face Patch*

Figure 7.15: *Graphical results to Table 7.3*

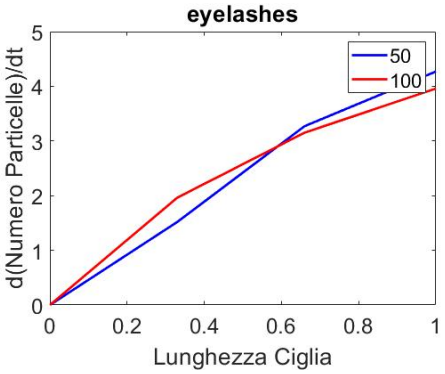


(a) *Eyelashes Patch*

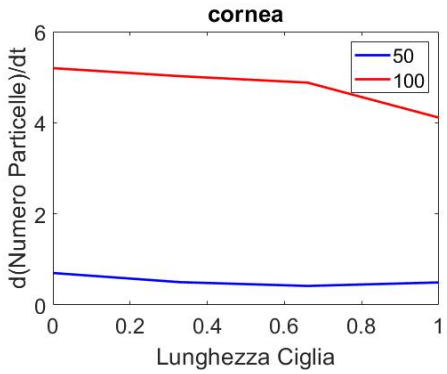


(b) *Cornea Patch*

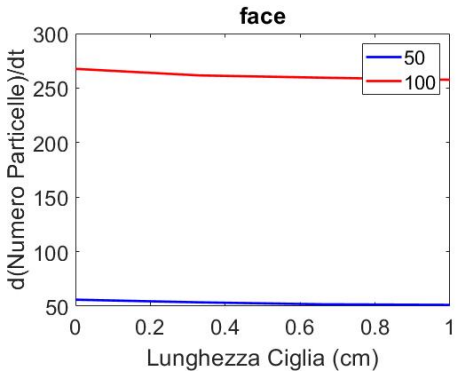


(c) *Face Patch*

Figure 7.16: *Comparative graphs relating to cases with particles with a fixed diameter of 50 and 100 $\mu m$*

The interesting result, as you can see from the *Figure* 7.16, is the trend of adhesion to the eyelashes. It is interesting to note how the trend of the two curves is particularly similar, further proof that enhances the decision to parameterize our study. As regards the cornea, but especially the face, the increase in inertia is such as to push the particles to adhere more easily to the two patches considered.

# Chapter 8

# Conclusions

Starting from the data extrapolated above, we can draw some conclusions. First of all, as concerning the generated flow field, it is appears uniform throughout the domain, except for the area near, where we see a variation of both pressure and velocity field.
The region we are mostly interested in is that near the eye. We notice several effects, as might have been expected, but what we need to focus on is first of all the role of the eyelashes interfering with the generation of the flow field. As we have shown in the *Figures* 7.3 and 7.4 the eyelashes not only have a protective function on the eye, by preventing a large number of particles from interfering with the ocular surface, but they perform this function by changing the flow field. This phenomenon is naturally more pronounced as the length of the lashes increases.
The study of conclusions relating to particles, on the other hand, is divided into two sections: the study of particles with normal diameter distribution and the study and comparison of particles with a fixed diameter.
The choice of analyzing particles with a normal distribution of diameter arises from the fact that in nature the particles do not have a fixed diameter. As it can be seen from the *Figure* 7.13, the particle deposition for the four eyelash lengths examined is homogeneous. Naturally, as the length of the eyelashes increases, the number of particles that they are able to intercept increases. This behavior is due to the combination of the two factors: the greater influence of longer eyelashes on the flow field and the effective greater length of a eyelash, which will inevitably intercept a greater number of particles. This affects particles deposition on the cornea: as the number of particles that are intercepted by the eyelashes increases, the number of particles that adhere to the cornea decreases. The discourse relat-

ing to the face patch is more isolated for the purposes of the discussion. Here, in fact, the protective function of the eyelashes was not expected to be predominant and actually it is not. In fact, the eyelashes protect only a small percentage of the surface of the face so they cannot be a total defense tool.
The analysis continued by studying the time derivatives of the number of particles that deposits on each patch. This is because, as shown in *Figures* 7.9, 7.10 and 7.11, the deposition of the particles on the various patches was actually approximable with a straight line. For this reason, the value of the time derivative of these lines on the various patches is approximately constant: the values obtained, shown in the *Table* 7.1 and subsequently graphed, therefore represent the number of particles adhering to the various surfaces per unit time.
Therefore, being able to study the trend of the derivatives of the normalized values, we have also been able to study this phenomenon in a more streamlined way, that is to say by considering a number of particles entering the system per second equal to just 5000. This is because we have considered the situation to be simulated with some simplifications: we did not take into account collisions between particles and the force of the particles on the flow itself.
The second case, on the other hand, the one with a fixed particle diameter, was studied with a different purpose. In fact, here we have not just one study, but two different fixed-diameter situations that allow us to compare the results to arrive to a single conclusion. This means that we are able to carry out what is called a parametric study, in which the results coming from the comparison of two different situations allow us to trace a trend that is supposed to be uniform even in cases differents than those analyzed. In particular, the results derived from the study of particles with a diameter of 50 and 100 $\mu$m, if related to each other, allow us to extrapolate a model that can also be applied to particles with finer or coarser particles. This allows for example to study PM10 in an appreciable way, that can be useful if we want to study the protection against viral agents such as Sars-CoV-2 as, as known by SIMA (Societa' Italiana di Medicina Ambientale), it is known that atmospheric particulate acts as a carrier, i.e. as a transport vector, for many chemical and biological contaminants, including viruses. Viruses "attach themselves" (with a process of coagulation) to atmospheric particulate, consisting of solid and / or liquid particles capable to remain in the atmosphere even for hours, days or weeks, and which can be transported over long distances. Atmospheric particulate matter, in addition to being a carrier, constitutes a substrate

that allows the virus to remain in the air in vital conditions for a certain time, in the order of hours or days. As can be seen from the *Figure* 7.16, the tendency of the particles to adhere varies according to the patch they encounter. As for the eyelash patch, we note a similar trend in the two curves at diameter 50 and 100 $\mu$m.

This result is important because it allows non-trivial conclusions. Having considered two particles with very different diameters, their tendency to adhere to the lashes remains similar. This justifies the hypothesis that this model can be extended to particles with an even smaller diameter. The protective function of the eyelashes in terms of barrier might therefore also be valid against potentially pathogenic particles such as PM10 or Sars-CoV-2. The speech related to the cornea patch does not differ much from the eyelash patch. Also in this case the trend of the adhesion is similar between the two different diameters. This supports even more the assumption expressed above on the eyelashes. If we consider the eyelashes area, where the mesh is more refined, we think the values are very similar in the two cases. It is therefore legitimate to assume that this tendency is also found in cases with particles with different diameters, in particular smaller ones such as PM10 or Sars-CoV-2. The analysis ends with the study of the face patch. This is the least relevant part of our discussion, as it covers a very large area, which minimally includes the eye. In each case, the results show significant differences in adhesion between cases with different diameters. However, this does not affect our analysis that much, as these considerations do not specifically concern the eye but, as mentioned, a much wider region.

The work presented is a new field of research and with many new possible developments and implications; it represents a solid basis for fully understanding the role of eyelash protection to the ocular surface. In this regard for future studies, that an interesting factor to be introduced could be the parameterization of two different elements: the diameter of the lashes and their curvature. This would help to create a model with a more realistic geometry. The hope is that such implementations will lead to an ever better understanding of the role of eyelashes in the defense against external pathogens.

# Bibliography


[1] Guillermo J Amador, Wenbin Mao, Peter DeMercurio, Carmen Montero, Joel Clewis, Alexander Alexeev, and David L Hu. Eyelashes divert airflow to protect the eye. *Journal of the Royal Society Interface*, 12(105):20141294, 2015.

[2] Web page: https://ancler.org/.

[3] Benjamin D Horne, Elizabeth A Joy, Michelle G Hofmann, Per H Gesteland, John B Cannon, Jacob S Lefler, Denitza P Blagev, E Kent Korgenski, Natalie Torosyan, Grant I Hansen, et al. Short-term elevation of fine particulate matter air pollution and acute lower respiratory infection. *American journal of respiratory and critical care medicine*, 198(6):759–766, 2018.

[4] Khursheed Ul Islam and Jawed Iqbal. An update on molecular diagnostics for covid-19. *Frontiers in cellular and infection microbiology*, 10, 2020.

[5] Yongjian Zhu, Jingui Xie, Fengming Huang, and Liqing Cao. Association between short-term exposure to air pollution and covid-19 infection: Evidence from china. *Science of the total environment*, 727:138704, 2020.

[6] Maria A Zoran, Roxana S Savastru, Dan M Savastru, and Marina N Tautan. Assessing the relationship between surface levels of pm2. 5 and pm10 particulate matter impact on covid-19 in milan, italy. *Science of the total environment*, 738:139825, 2020.

[7] Web page: https://www.isprambiente.gov.it/.

[8] Richard J Braun. Dynamics of the tear film. *Annual Review of Fluid Mechanics*, 44:267–297, 2012.

[9] JI Na, OS Kwon, BJ Kim, WS Park, JK Oh, KH Kim, KH Cho, and HC Eun. Ethnic characteristics of eyelashes: a comparative analysis in asian and caucasian females. *British Journal of Dermatology*, 155(6):1170–1176, 2006.

[10] Barry D Kels, Andrzej Grzybowski, and Jane M Grant-Kels. Human ocular anatomy. *Clinics in dermatology*, 33(2):140–146, 2015.

[11] Web page: http://www.medicalook.com/human$_a$*natomy/organs/eyelids$_a$nd$_e$yelashes.htr*

[12] Web page: https://www.blender.org/.

[13] Web page: https://cfd.direct/.

[14] Web page: https://www.openfoam.com/.

[15] Bjarne Stroustrup. *The C++ programming language*. Pearson Education India, 2000.

[16] Fadl Moukalled, L Mangani, Marwan Darwish, et al. *The finite volume method in computational fluid dynamics*, volume 113. Springer, 2016.

[17] G Biswas and V Eswaran. *Turbulent flows: Fundamentals, experiments and modeling*. CRC Press, 2002.

[18] Philippe R Spalart. Strategies for turbulence modelling and simulations. *International journal of heat and fluid flow*, 21(3):252–263, 2000.

[19] Web page: https://www.wolfdynamics.com.

[20] Joel Guerrero. Introduction to computational fluid dynamics: Governing equations, turbulence modeling introduction and finite volume discretization basics. *Predavanja, Veljača*, 2014.

[21] Web page: https://knowledge.autodesk.com/it/support/simulation-mechanical/learn-explore/caas/sfdcarticles/sfdcarticles/ita/how-to-perform-a-mesh-convergence-study.html.

[22] Said Elghobashi. On predicting particle-laden turbulent flows. *Applied scientific research*, 52(4):309–329, 1994.

[23] E Loth. Numerical approaches for motion of dispersed particles, droplets and bubbles. *Progress in energy and combustion science*, 26(3):161–223, 2000.

[24] Clayton T Crowe and Efstathios E Michaelides. Basic concepts and definitions. *Multiphase flow handbook*, pages 24–25, 2006.

[25] X Xie, Y Li, ATY Chwang, PL Ho, and WH Seto. How far droplets can move in indoor environments-revisiting the wells evaporation-falling curve. *Indoor air*, 17(3):211–225, 2007.